Spatial and temporal distributions of polycyclic aromatic hydrocarbons in sediments from the Canadian Arctic Archipelago

Anne Corminboeuf [1,*], Jean-Carlos Montero-Serrano [1], Richard St-Louis [2]

[1] Institut des sciences de la mer de Rimouski (ISMER), Université du Québec à Rimouski, 310 Allée des Ursulines, Rimouski, QC, G5L 3A1, Canada

[2] Université du Québec à Rimouski, 300 Allée des Ursulines, Rimouski, QC, G5L 3A1, Canada

* Corresponding author: A. Corminboeuf; annecorminboeuf@hotmail.com

Highlights

- The polycyclic aromatic hydrocarbon (PAH) concentrations in Canadian Arctic sediments are low
- The PAH input to sediments has remained constant throughout the last century
- The PAHs in Canadian Arctic sediments mainly originate from natural sources

Abstract

1. The concentrations of 23 polycyclic aromatic hydrocarbons (PAHs; 16 parent and 7 alkylated PAHs) in 113 surface marine sediment samples, 13 on-land sediment samples and 8 subsampled push cores retrieved from the Canadian Arctic Archipelago (CAA) were calculated. PAHs were extracted via accelerated solvent extraction (ASE) and quantified via gas chromatography-mass spectrometry (GC-MS). The sums of the concentrations 16 PAHs in the surface sediments ranged from 7.8 to 247.7 ng g^{-1} (dry weight [dw]) basis). The PAH inputs to the sediments have remained constant during the last century and agree with the results obtained for the surface sediments. Diagnostic ratios indicated that the PAHs in the CAA mainly originate from natural petrogenic sources, with some pyrogenic sources. Temporal trends did not indicate major source shifts and largely indicated petrogenic inputs. Overall, the sediments retrieved from the CAA have low PAH concentrations that are mainly natural.

Keywords: Canadian Arctic Archipelago, sediments, polycyclic aromatic hydrocarbons, baseline, pollution, Late Holocene.

1. Introduction

Within the context of climate change, the Arctic is undergoing major perturbations, and many studies have focused on sea ice conditions and navigability projections in the Arctic Ocean (Lasserre *et al.,* 2010; Askenov *et al.,* 2017). Because the summer sea ice extent is rapidly decreasing, leading to a seasonally ice-free Arctic Ocean, it has been speculated that maritime traffic could increase within the Canadian Arctic Archipelago (CAA); for example, the northwest passage could open to cargo transportation for a longer time period each year by the middle of the century (Lasserre *et al.,* 2010; Smith and Stephenson, 2013). This shipping route connecting Asia and Europe is shorter than the Suez Canal, the Panama Canal or the Cape of Good Hope (Lasserre *et al.,* 2010; Askenov *et al.,* 2017). Hence, maritime companies have shown interest in traveling through the Arctic since this would allow time and fuel savings and consequent cost reductions. However, maritime traffic and oil exploration within the Arctic could also increase the anthropogenic pressure and pollution load in Arctic ecosystems (Jörrundsdóttir, 2014).

Shipping-related fuel combustion and anthropogenic activities are local sources of polycyclic aromatic hydrocarbons (PAHs), which constitute a wide class of organic compounds consisting of more than one benzene ring (C_6H_6) fused in a variety of conformations (AMAP, 2017; Haritash and Kaushik, 2009). Hundreds of these compounds are found in the environment, but since the mid-70s, 16 PAHs have been listed as priority environmental pollutants by the Environmental Protection Agency of the United States (US EPA) and are therefore closely monitored (Keith *et al.,* 2014; Pampanin and Sydnes, 2017). Hence, PAHs are pollutants of great concern, especially since the emissions originating in developed countries have decreased while those originating in developing countries have increased (Zhang and Tao, 2009; Wang *et al.,* 2010).

PAHs are introduced to the environment via natural or anthropogenic sources (Lima *et al.*, 2005; Foster *et al.,* 2015; Chen *et al*., 2018), and anthropogenic activities are major sources of the PAHs occurring in the biosphere (Yanik *et al.,* 2003; Morillo *et al.,* 2008). Seven PAHs have been classified as probably carcinogenic for humans by the International Agency for Research on Cancer (IARC) of the World Health Organization because of the reactivity of their metabolites (IARC, 1987). Inuit communities within the Arctic might be exposed to PAHs via the consumption of traditional foods such as mollusks (Rapinski *et al.,* 2018). However, the Arctic is a region where the seafloor composition is the least studied and understood. Indeed, the vast majority of the channels within the CAA and their adjoining continental shelves and slopes exhibit a substantial knowledge gap regarding sediment composition and associated contaminants (Stein, 2008). Moreover, studies have focused on specific areas of the Arctic (e.g., Beaufort Sea or Baffin Bay; Yunker *et al.,* 1995, 2002a, 2002b; Foster *et al.,* 2015) or sites near anthropogenic influences (Boitsov *et al.,* 2009a,b; Zaborska *et al.,* 2011). To our knowledge, no complete baseline information on the PAHs in recent sediments or historic tendencies of the PAH inputs to sediments are available within the CAA.

2. Sources of the PAHs and their environmental fate within the CAA

2.1. PAH sources

Pyrogenic PAHs are produced during the incomplete combustion of organic matter, which includes forest and bush fires and fossil fuel and coal combustion (Chen *et al.,* 2018; Yu *et al.,* 2019). These PAHs are mainly emitted into the atmosphere and could occur either in the gaseous phase or bonded to the particulate phase (i.e., mineral dust and salt) (Tobiszewski and Namieśnik, 2012). Owing to their low vapor pressures, the majority of these semivolatile compounds undergoes repeated cycles of volatilization-deposition, travel across long distances and eventually end up in waters, soils and sediments via deposition (AMAP, 2017; Chen *et al.,* 2018; Balmer *et al.,* 2019). The PAHs produced at mid-latitudes

could thus reach the Arctic, as shown by modeling studies (Wang *et al.,* 2010; Sofowote *et al*., 2011).

Petrogenic PAHs are hydrocarbons stemming from losses or seepage of oil and petroleum deposits, crude oil spills or rock weathering and are therefore naturally present in sediments and water bodies, and these PAHs are not of great concern because of their very low concentration (Lima *et al.,* 2005; Pampanin and Sydnes, 2017; Chen *et al.,* 2018). They are readily dispersed via water runoff, and since petrogenic PAHs are not directly emitted into the atmosphere, they are slightly influenced by long-range atmospheric transport (Pampanin and Sydnes, 2017).

2.2. Environmental fate

In the Arctic, PAHs stemming from distant sources may enter the marine environment via river discharge, but atmospheric long-range transport is believed to be a significant input process (Sofowote *et al.,* 2011; Yu *et al.,* 2019). Regarding the environmental fate of atmospheric PAHs, Lammel *et al*. (2009) showed via a modeling approach that between 0.5% and 12.8% of the total environmental burden of PAHs might be stored within Arctic ecosystems (i.e., air, soil, vegetation and ocean) depending on the chosen gas/particle partitioning scenario. In addition to the already existing natural PAHs in Arctic soils and sediments, atmospheric deposition of PAHs originating from remote sources, in addition to new local sources such as ship traffic and oil exploration/exploitation, are PAH sources in the CAA (Balmer *et al.,* 2019). PAHs are not easily degraded under natural conditions and are therefore slightly persistent (Pelletier *et al.,* 2008; Haritash and Kaushik, 2009). Photooxidation of PAHs is a chemical pathway of degradation, but biological degradation by bacteria, fungi and algae is accepted as the main process (Roslund *et al.,* 2018; Haritash and Kaushik, 2009; Balmer *et al.,* 2019). Because most vertebrates (e.g., fishes, birds and mammals) readily metabolize PAHs, they do not tend to experience biomagnification through the food chain (Xue et Warshawsky, 2005; Haritash et Kaushik, 2009; AMAP, 2017). However, PAHs could accumulate in benthic species such as clams and mussels (Balmer *et al.* 2019), and these organisms are an important food source for northern

communities (Jörrundsdóttir *et al.*, 2014; Rapinski *et al.* 2018). If deposited on land, PAHs could leach through soils or could be transported via water runoff and eventually reach aquatic ecosystems (Wang *et al.*, 2007; Klungsøyr *et al.*, 2010). They are poorly soluble in water because of their hydrophobicity and lipophilicity (Chen *et al.*, 2018; Zhao *et al.*, 2016). Consequently, PAHs exhibit a relatively high affinity for suspended and particulate matter and sediments, which is why the latter are considered the main sink of PAHs (Chen *et al.*, 2018).

Considering that PAHs are pollutants of interest that could be released by an increase in anthropogenic activities in the Arctic and that could accumulate in sediments and considering that the Arctic sediment PAH composition is not completely known, it is essential to determine the actual baseline. The aim of this study is to (1) characterize the modern spatial distribution patterns of the PAHs within the CAA, (2) determine the temporal trends of the PAH concentration based on ^{210}Pb-dated box cores collected across the CAA, and (3) establish the origin of PAHs (i.e., petrogenic or pyrogenic) according to two diagnostic ratios, namely, fluoranthene over the sum of fluoranthene and pyrene (Fla/[Fla+Pyr]) and benz(a)anthracene over the sum of benz(a)anthracene and chrysene (BaA/[BaA+Chr]).

3. Materials and methods

3.1 Study site

Since pyrogenic PAHs traveling via long-range atmospheric transport are deposited in soil or water and petrogenic PAHs mainly originate from rock weathering and oil reserves, they both occur in sediments, i.e., sediments are a sink for organic pollutants such as PAHs, and their affinity for fine and organic-rich sediments is well documented (Chiou *et al.*, 1998; Gschwend and Hites, 1981; Stark *et al.*, 2003). Letaïef (2019) reported that the sediments within the CAA ranged from clay (2 µm) to fine silt (4 to 8 µm). The total organic carbon (TOC) content is lower than 2% in most surface sediments retrieved from the CAA (e.g.,

Letaïef, 2019). More specifically, the Mackenzie Shelf and Delta and the Beaufort Sea/Canada Basin exhibit TOC values ranging from 0.5% to 1.9% (Yunker *et al.*, 2011; Letaïef, 2019). The Queen Maud Gulf and the M'Clintock Channel, central CAA, exhibit relatively low TOC contents, with values ranging from 0.2% to 0.5 % (Letaïef, 2019). Finally, the TOC content in Baffin Bay sediments ranges from 0.2% to 1.5% (Stein, 1991; Madaj, 2016). The CAA counts approximately 36500 islands and numerous waterways, straits, channels and sills formed by glacial action under past climate conditions (Melling *et al.*, 2002; Michel *et al.*, 2006). The recent sedimentary dynamics within the CAA are controlled by the sediment supply stemming from river discharge in the west and central CAA, whereas the east CAA is more influenced by sea ice and coastal erosion (Letaïef, 2019). Indeed, the Mackenzie River alone annually discharges approximately 420 km^3/yr of sediments onto the continental shelf of the Beaufort Sea and is therefore a major source of continental PAHs (Wagner *et al.*, 2011). Other small rivers exert a cumulative significant impact on the sediment load, such as the Coppermine River, the Ellice and Back Rivers and the Cunningham River, with a total contribution of approximately 110 km^3/yr (Alkire *et al.*, 2017). Once in the marine ecosystem, sediments are entrained throughout the archipelago by sea ice via suspension freezing and ice anchoring (Reimnitz *et al.*, 1993; Darby *et al.*, 2003, 2011; Stein, 2008). Coastal erosion by seasonal sea ice, glaciogenic debris flows, meltwater plumes, mass movements along submarine canyons and sea lifting are other dominant sedimentary processes in glacial environments contributing to the dispersal of sediments across great distances within the CAA (Hiscott *et al.*, 1989; Ó Cofaigh *et al.*, 2003; Harris, 2012; Dowdeswell *et al.*, 2015; Lai *et al.*, 2016). Processes involving sea ice are mostly active during the sea ice formation season, and sediments are discharged elsewhere during summer melting (Darby *et al.*, 2011). All of these processes contribute to the dispersion of PAHs originating from distant sources within the CAA before they become trapped in marine sediments.

3.2 Materials and reagents

All reagents were of analytical or high-performance liquid chromatography (HPLC) grade. Hexanes and dichloromethane were obtained from Anachemia, methanol was acquired from Millipore and 2-propanol was obtained from Fisher Chemicals. Nitric acid (HNO_3) and hydrochloric acid (HCl) were acquired from VWR Analytical. Silica gel (technical grade, 70-230 mesh) and copper powder (<425 µm) were obtained from Sigma-Aldrich. Diatomaceous earth (celite 566) was acquired from UCT Enviro-Clean. Standard reference material NIST-1944 was purchased from the National Institute of Standards and Technology (NIST). PAH Mix manufactured by AccuStandard was adopted for the generation of calibration curves, combined with an alkylated PAH homemade mix (2,6-dimethylnaphthalene and 9,10-dimethylanthracene were obtained from Sigma-Aldrich, while 2,3,5-trimethylnaphthalene, 1-methtylnaphthalene and 3,6-dimethylphenanthrene were acquired from Fisher Chemicals). Before analysis, every sample was spiked with deuterated 1-methylnaphthalene and benz(a)anthracene purchased from Sigma. A mixture of deuterated naphthalene (Sigma-Aldrich), anthracene (Cambridge Isotope Laboratories) and perylene (Sigma-Aldrich) was added as an internal standard for quantification purposes. The targeted compounds in this study included 16 parent PAHs and 7 alkylated PAHs: naphthalene, 1-methylnaphthalene, 2-methylnaphthalene, 2,6-dimethylnaphthalene, acenaphthylene, acenaphthene, 2,3,5-trimethylnaphthalene, fluorene, phenanthrene, anthracene, 1-methylphenanthrene, 3,6-dimethylphenanthrene, fluoranthene, pyrene, 9,10-dimethylanthracene, benz(a)anthracene, chrysene, benzo(b)fluoranthene, benzo(k)fluoranthene, benzo(a)pyrene, indeno(1,2,3-c,d)pyrene, dibenz(a,h)anthracene and benzo(g,h,i)perylene.

Silica gel was activated at 450°C for 2 h and stored in a desiccator. Copper powder, for sulfur removal from sediments, was activated as follows: in a Teflon tube, copper powder was covered with hydrochloric acid (HCl) 6N and shaken for 3 min. It was then rinsed with distilled water until a neutral pH was attained. The copper powder was then washed 3 times

with both methanol and dichloromethane and was finally stored in a Teflon tube covered with dichloromethane.

3.3 Sediment samples and chronology

A total of 126 sediment samples was analyzed in this study: 113 marine surface sediment samples and 13 terrestrial sediment samples collected from glaciers and rivers (Fig. 1). Additionally, 8 push cores were subsampled to determine temporal trends (Fig. 1). All samples were retrieved from box cores collected between 2016 and 2019 across a large area covering the Canadian Beaufort Sea to Baffin Bay during the ArcticNet summer expeditions onboard the Canadian Coast Guard Ship (CCGS) icebreaker Amundsen. Samples were collected from glaciers and rivers using the ship helicopter as CCGS Amundsen traveled through the CAA. All marine coring sites were targeted using high-resolution seismic profiles, which indicated that Late Holocene sediment accumulation was not influenced by mass wasting events (Montero-Serrano *et al.*, 2016, 2017, 2018, 2019).

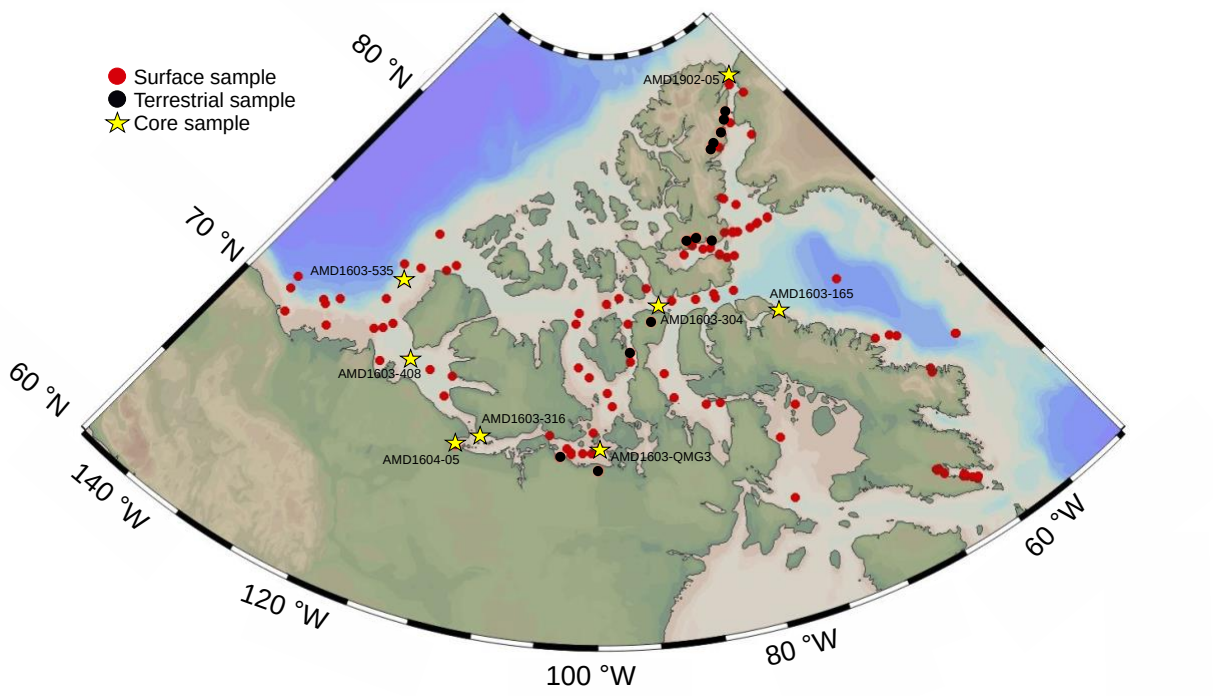

Fig. 1 Locations of the sediment samples collected from the Canadian Arctic Archipelago.

Surface sediments (uppermost 0.5 to 1 cm) were collected with a spoon and stored in plastic bags (WhirlPack) at 4°C until further analysis. Push cores were collected by pushing a plexiglass tube (10-cm diameter) into sediments. The cores were stored at 4°C until further subsampling. Sediment subsamples were retrieved from the push cores from 0 to 10 cm at 1-cm intervals. Age-depth models of the box cores have been previously published in Letaïef (2019), constructed using ^{210}Pb measurements combined with the constant rate of supply (CRS) model (a constant rate of the ^{210}Pb supply; Appleby and Oldfield, 1983). The age is reported as common era (CE) and before common era (BCE) hereafter. The sedimentation rates and ages at ~10 cm depth are provided in Table 1 and Fig. S1. Note that no dates are available for core AMD1902-05BC recovered in the Robeson Channel (Fig. 1). However, based on the sedimentation rate (4 cm ka^{-1}) determined for a well-dated neighboring core (HLY03-05GC; Jennings *et al.*, 2011), we inferred that the age at a core depth of ~10 cm is approximately 2.5 cal ka BP (550 BCE).

Table 1. Sedimentation rate and sediment age at ~10 cm of the push cores used in this study.

Core ID	Sedimentation rate (cm ka^{-1})	Age (~10 cm of core depth)
AMD1604-05BC	178	1956 CE
AMD1603-165BC	82	1894 CE
AMD1603-304BC	184	1962 CE
AMD1603-316BC	111	1926 CE
AMD1603-408BC	87	1901 CE
AMD1603-535BC	113	1928 CE
AMD1603-QMG4BC	164	1955 CE
AMD1902-05BC	4*	550 BCE

* Sedimentation rate inferred from Jennings *et al.* (2011).

All samples were sieved through a 150-µm Nitex® mesh using distilled water. The <150 µm sediment fraction was then stored in a 50-mL Falcon® tube successively rinsed with tap water and soap, distilled water, nitric acid (HNO_3) 5% (3 times), distilled water and 2-propanol (3 times). The sediment samples were then frozen at -80°C for at least 12 h and freeze dried. The samples were finally crushed using an agate mortar. Aliquots weighing 5 g of these homogenized sediment samples were used for PAH analysis.

3.4 PAH extraction and analysis

PAH extraction was conducted via accelerated solvent extraction (ASE) following the method developed by Choi *et al.* (2014). Briefly, 22-mL stainless-steel extraction cells were loaded as follows, from bottom to top: cellulose filter, diatomaceous earth, activated silica gel (5 g), activated copper (5 g), freeze-dried sediment sample (5 g) and diatomaceous earth to the top (Fig. S2). A PAH spike (1-methylnaphthalene-d10 and benz(a)anthracene-d12) was directly added onto the sediment sample. The cells were maintained open and protected from dust contamination at room temperature for 2 h to acclimate. Blanks were prepared similar to the samples but with no sediments. To confirm the accuracy of the method, 0.5 g of standard reference material NIST-1944 was processed as a sample. One blank, one standard reference material sample and one duplicate were tested for every 12 samples.

The addition of activated silica gel and copper directly to the cell enabled one-step extraction and cleanup. The extraction was performed with a Dionex ASE 200 system (Thermo Co., Sunnyvale, CA, USA). The temperature and pressure were set to 100°C and 1700 psi, respectively. The flush volume and purge time were set to 60% and 100 s, respectively. The extraction was performed with a mixture of hexane and dichloromethane (at a ratio of 4:1 v/v) and two static cycles of 5 min. Extracts were collected in 60-mL clear collection vials (previously rinsed with tap water and soap, distilled water, hexane and dichloromethane (4:1 v/v) mixture and propanol). The extracts were then evaporated to approximately 5 mL with a rotating evaporator and then evaporated to exactly 0.5 mL with a nitrogen stream at room temperature. In regard to standard material NIST-1944, the extracts were evaporated to exactly 1.5 mL.

PAH analysis was performed via gas chromatography (GC, Agilent Technologies 6850 series II; Santa Clara, CA, USA) coupled with mass spectrometry (MS, Agilent Technologies 5975B VL MSD) using total ion count (TIC). The injection was performed with an Agilent Technologies 6850 series autosampler. The capillary column used was an Rxi®-5 ms (30 m x 0.25-mm inner diameter (ID) x 0.25 µm ft, 5% diphenyl and 95%

polysiloxane from RESTEK). The oven temperature was set as follow: 50°C for 2 min, 15°C/min until 275°C, held for 2 min, 15°C/min until 325°C, held for 15 min, and a postrun of 2 min at 300°C. A sample volume of 1 µL was injected at a temperature of 250°C under splitless injection with helium as the carrier gas at a flow rate of 1 mL/min.

3.5 Quality control and quality assurance (QC/QA)

The procedural blanks did not reveal contamination. Hence, the results were not blank corrected. The spike recoveries were 73.7% ± 15.0% for 1-methynaphthalene-d10 and 83.5% ± 23.2% for benz(a)anthracene-d12. Some samples did not meet the generally accepted QC/QA recovery criteria of 70% to 103%. All samples were hence spike corrected. The efficiency of the method was confirmed with standard reference material NIST-1944. The mean recoveries obtained are compared in Table S2 to those obtained by Choi *et al.* (2014), who developed the ASE method applied in this study. The method detection limit (MDL) for each PAH was calculated as suggested by the US EPA (Oblinger Childress *et al.*, 1999). Briefly, 7 replicates of a spiked solution at the second lowest calibration point were analyzed. Hence, the MDL was determined as 3.143 times (Student's *t* value for 6 degrees of freedom and the 99% confidence level) the standard deviation of the measured concentration for each compound. The MDL ranged from 8.1 ng/g for benz(a)anthracene to 155.9 ng/g for acenaphthylene (Table S2).

3.6 Data processing

Prior to all multivariate analyses, the values below the detection limit (VBDLs) were imputed via multiplicative lognormal replacement with R package zCompositions (Palarea-Albaladejo and Martin-Fernandez, 2015). This method preserves the geometry of the compositional data while accounting for corresponding detection limit thresholds. However, variables with VBDLs greater than 30% [such as acenaphthylene, 2,3,5-trimethylnaphthalene, benz(a)anthracene, benzo(b)fluoranthene, benzo(k)fluoranthene, benzo(a)pyrene, indeno(1,2,3-c,d)pyrene, dibenz(a,h)anthracene, and benzo(g,h,i)perylene] were omitted in the subsequent multivariate analyses (Palarea-

Albaladejo and Martin-Fernandez, 2015). Next, a log-centered (clr) transform was applied to the data (Aitchison, 1990). This operation removed the statistical constraints on the compositional variables, such as the constant-unit sum, and enabled the valid application of classical (Euclidean) statistical methods to the compositional data (Aitchison, 1986, 1990; Montero-Serrano *et al.,* 2010). We applied fuzzy c-means (FCM) clustering analysis (Kaufman and Rousseeuw, 2009) to identify samples possessing similar PAH compositions within the CAA. We adopted the Aitchison distance as a measure of similarity between the samples and the Ward method (minimum-variance method) for agglomerative calculation purposes. The FCM algorithm requires in-advance specification of the overall number of clusters to be detected. R package NbClust (Charrad *et al.*, 2014) was employed to apply 23 indices and to determine the optimum number of clusters. The FCM clustering results are visualized in silhouette and principal coordinate ordination plots (Kaufman and Rousseeuw, 2009). The silhouette plot allows visualization of the robustness of clusters, where negative values indicate an incorrect and/or questionable assignment (Borcard *et al.*, 2011). Moreover, principal component analysis (PCA) was performed using the PAH data and FCM clustering results with the goal of determining PAH associations with similar relative variation patterns (von Eynatten *et al.,* 2003; Montero-Serrano *et al.,* 2010). FCM clustering analysis was conducted with R software (R Core Team, 2020) using the compositions (van den Boogaart and Tolosana-Delgado, 2008) and cluster packages (Maechler *et al.,* 2019). PCA was conducted with Compositional Data Package (CODAPAK) software (Comas and Thió-Henestrosa, 2011). Finally, the FCM clustering results and PAH concentrations were analyzed to produce distribution maps using Ocean Data View software (Schlitzer, 2015). These maps were generated using a weighted-average gridding algorithm with a quality limit of 1.5. Diagnostic ratios of fluoranthene over the sum of fluoranthene and pyrene (Fla/[Fla+Pyr]) and benz(a)anthracene over the sum of benz(a)anthracene and chrysene (BaA/[BaA+Chr]) were considered to draw boxplots and discriminate PAH sources (i.e., pyrogenic vs petrogenic).

4. Results and discussion

4.1. FCM clustering analysis

The FCM clustering analysis results indicate that there are three regional PAH clusters within the CAA (Figs. 2A and S3). Cluster 1 (PAH C#1, red) is mostly representative of the western CAA. Yunker *et al.* (1996) showed that the Mackenzie River imposed a dominant influence on the sedimentary dynamics in this region, namely, all their samples collected from the Mackenzie River, the Mackenzie Shelf and the Beaufort Sea Shelf edge clustered together, agree with our results. This cluster also seems to be dominated more by both medium molecular weight PAHs (MMW = 4-5 rings) and light molecular weight PAHs (LMW = 2-3 rings). This cluster exhibits a higher influence of high molecular weight PAHs (HMW= 6 rings) than the other clusters; however, HMW PAHs are minor contributors to the clusters (Fig. 2B). Clusters 2 (PAH C#2, green) and 3 (PAH C#3, blue) are slightly less defined. However, cluster 2 tends to be more represented by LMW PAHs and samples from the eastern CAA, while cluster 3 is more represented by LMW to MMW PAHs (and samples retrieved from the central CAA, as shown in Fig. 2B).

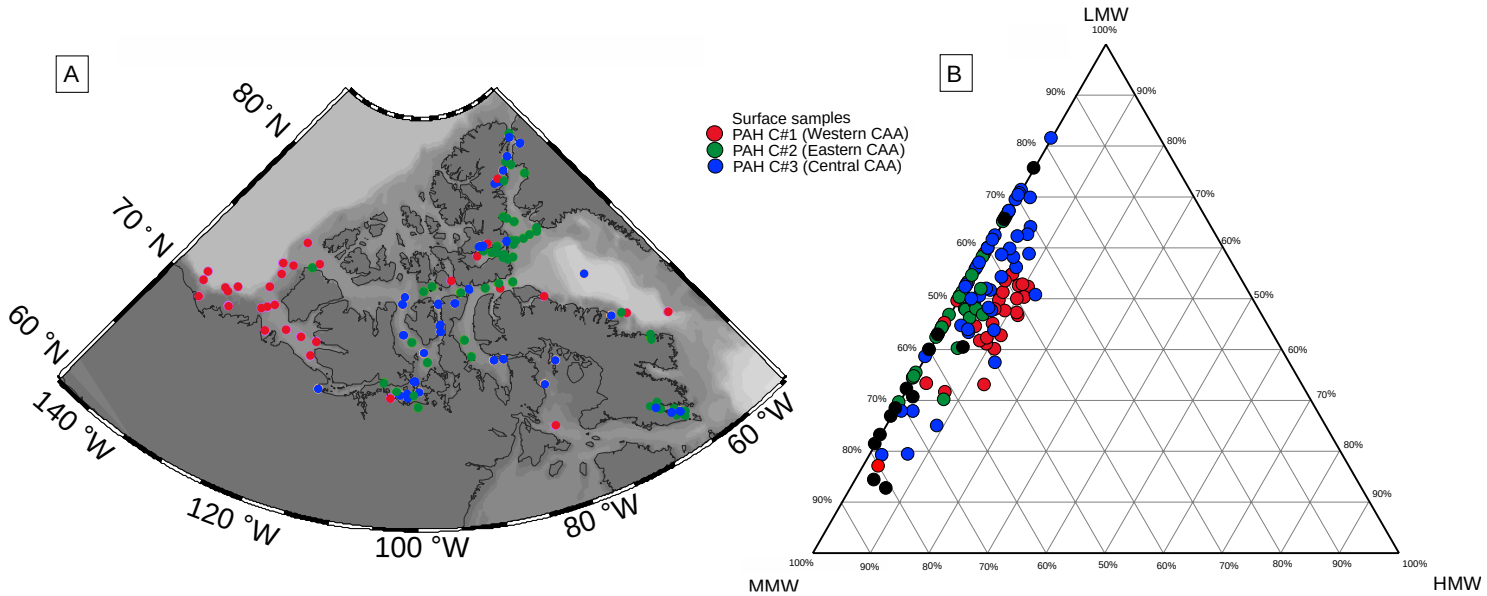

Fig. 2. (A) Fuzzy clustering results for the surface samples and (B) ternary diagram for the surface and terrestrial samples (black dots) regarding low-molecular weight (LMW, 2-3 rings), medium-molecular weight (MMW, 4-5 rings) and high-molecular weight (HMW, 6 rings) parent PAHs.

The ordination diagram (Fig. 3A) and silhouette plot (Fig. 3B) show the robustness of the above clusters, revealing that the samples can be divided into 3 clusters: (1) western CAA, (2) eastern CAA and (3) central CAA. The negative values in Fig. 3B indicate an incorrect and/or questionable assignment. The second group contains the most samples (n=6) that might belong to another group, whereas only 3 samples of the other groups might be incorrectly assigned. Indeed, those samples show a greater mix between the 3 clusters, likely due to their PAHs assemblages and sources (Fig. S4).

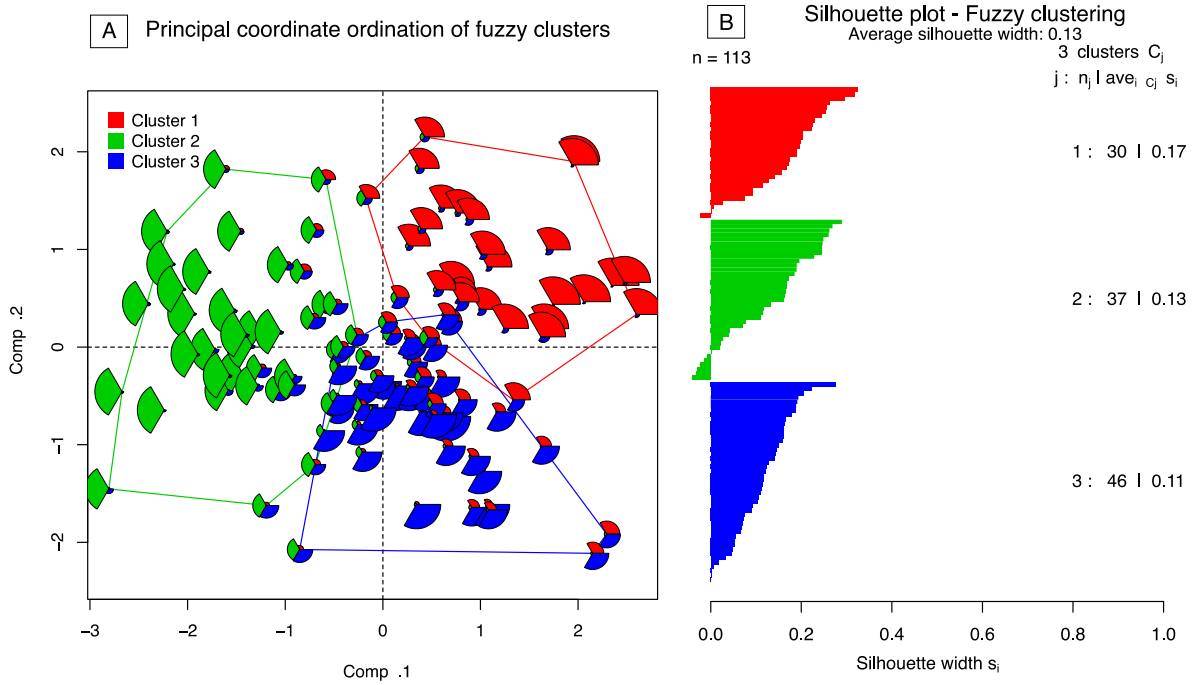

Fig. 3. (A) Ordination of the fuzzy clusters (principal coordinate analysis, PCoA) and (B) silhouette plot for fuzzy clustering of the surface samples based on the PAH concentration. The number of samples per cluster and their membership values are listed on the right-hand side of Fig. 6B.

4.2. Distribution of the PAHs in recent sediments

The sums of the concentrations of the 16 priority PAHs (Σ_{16}PAHs, dry weight [dw]) designated by the US EPA in the surface sediments of the CAA ranged from 7.8 to 247.7 ng g^{-1} with a mean value of 56.8 ng g^{-1} (Fig. 4B; Table 2). The highest values of Σ_{16}PAHs are

found in the western CAA, with values ranging from 15.7 to 247.7 ng g^{-1} and a mean value of 107.9 ng g^{-1} (Fig. 4B).

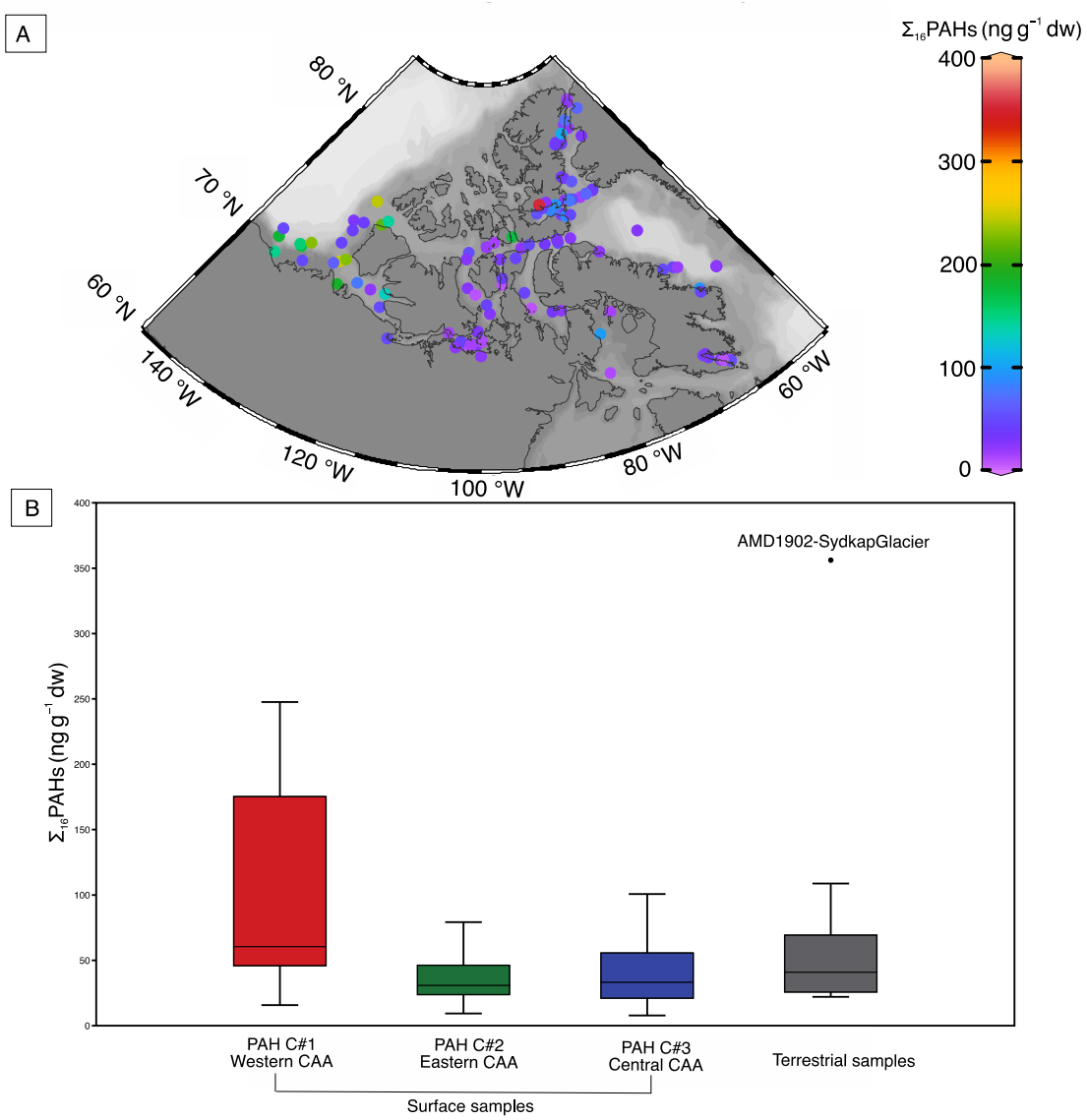

Fig. 4. (A) Spatial distribution of Σ_{16}PAHs (ng g^{-1} dw) in the surface and terrestrial samples of the CAA and (B) box plots of Σ_{16}PAHs (ng g^{-1} dw) separated by cluster.

According to the values reported in the literature (Table 2), it seems that the seafloors near the Mackenzie River are naturally rich in PAHs, which has been previously explained by the river discharge of the Mackenzie River (Yunker *et al.*, 2002a). Indeed, the river alone discharges an annual flux of 49 ± 8 tons of both particulate and dissolved PAHs onto the

Mackenzie Shelf (Yunker *et al.*, 1991). Additionally, the western CAA is well known for three areas of natural hydrocarbon seeps (oil and/or gas) along the Mackenzie River, Delta and Shelf (Thomas, 1979; Janicki, 2001; Yunker *et al.*, 2002a). The Beaufort Shelf and Mackenzie Shelf are also known for their pockmarks and mud volcanoes releasing fluids and gas into the water column (Blasco *et al.*, 2006; Walsh *et al.*, 2006). Certain on-land seeps, such as the Smoking Hills (Cape Bathurst, Northwest Territories), also release smoke clouds and fumaroles containing PAHs that are then transported by wind (Klungsøyr *et al.*, 2010). The western CAA also has a past history of petroleum exploration. Indeed, from the 1960s to the 1990s, extensive drilling was performed in the Mackenzie/Beaufort Basin, and many sumps for drilling wastes were built, which have leaked since their abandonment. Hence, accidental oil spills have occurred, but the total inputs are much lower than those from other sources (Klungsøyr *et al.*, 2010). This natural hydrocarbon-rich background and petroleum exploration/extraction activity could explain the relatively high concentrations observed in the Mackenzie River area. Overall, the surface sediment concentrations of Σ_{16}PAHs reported in other studies for the Canada Basin (58.9 – 75.9 ng g^{-1}; Ma *et al.*, 2017) and the Chukchi Sea/Canada Basin (102 ng g^{-1}; Yunker *et al.*, 2011 and 8.8 – 78.3 ng g^{-1}; Ma *et al.*, 2017) are comparable to those reported here for the western CAA but lower than those reported for the Mackenzie Shelf (495 – 755 ng g^{-1}; Yunker and MacDonald, 1995).

Table 2. Comparison of the Σ_{16}PAH values of the US EPA in the marine sediments of the CAA and other Arctic regions

Region	$\sum_{16}$PAHs (ng g^{-1} dw)	Reference
Chukchi Plateau Makarov Basin	41.6 2.0	Dong *et al.*, 2015
Canada Basin Chucki Sea Central Arctic Ocean	58.9 – 75.9 (68.3) 8.8 – 78.3 (49.7) 5.8 – 33.9 (13.07)	Ma *et al.*, 2017
North Baffin Bay	25.6 – 199.4 (105.9)	Foster *et al.*, 2015
Beaufort Sea/Canada Basin Chukchi Sea/Canada Basin Mackenzie Shelf Mackenzie Shelf Edge	412 102 755 495	Yunker *et al.*, 2011
Canada Basin	27.66 – 167.48	Chen *et al.*, 2018
Canada Basin Makarov Basin	71.4 – 150.2 (115.7) 36.9 – 74.2 (59.5)	Zhao *et al.*, 2016
Kara Sea	ND - 110	Sericano *et al.*, 2001
Svalbard coastal sediments	25 - 38	Jiao *et al.*, 2009
Barents Sea	31.6 – 245.2 (114.3)	Boitsov *et al.*, 2009b
Western CAA Central CAA Eastern CAA Total CAA Terrestrial sediments	15.7 – 247.7 (107.9) 7.8 – 100.7 (40.8) 9.3– 79.2 (35.5) 7.8 – 247.7 (56.8) 22.1– 108.8 (71.1)	This study

Note: mean values, if available, are in parentheses.

In the two other regions of the CAA, the value of Σ_{16}PAHs (dw) remains low: 7.8 to 100.7 ng g^{-1} with a mean value of 40.8 ng g^{-1} for the eastern CAA and 9.3 to 79.2 ng g^{-1} with a mean value of 35.5 ng g^{-1} for the central CAA (Fig. 4B). These results are similar to other Arctic regions, such as the Kara Sea, the Barents Sea or the Svalbard coast, but higher than the reported values for the Makarov Basin or the Central Arctic Ocean (Table 2). Dong *et al.* (2015) pointed out a decreasing tendency of the PAH concentration with increasing latitude, which could explain why higher PAH concentrations occur in the CAA than those at other northerly sites (e.g., the Canada and Makarov Basins). Another known hydrocarbon seep is located in the eastern CAA along Baffin Island at Scott Inlet (Levy, 1978), but the sample collected near this area does not exhibit a higher concentration than those exhibited by the other samples collected from the eastern CAA. The values of Σ_{16}PAHs (dw) for the

terrestrial samples (i.e., glacier and river samples) are consistent with those for the marine sediments, with values ranging from 22.1 to 108.8 ng g^{-1} and a mean value of 71.1 ng g^{-1} (Fig. 4B), which are fairly low values. However, a major exception of 356.1 ng g^{-1} is found for the sample collected near the Sydkap Glacier, located approximately 60 km west of the Grise Fiord, the northernmost Inuit community in the CAA (Fig. 4A). It is the highest result among all the samples. No anthropogenic activities or historical accidental spills have been recorded in this area. However, Ellesmere Island is known for its numerous coal deposits (Ricketts and Embry, 1984; Kalkreuth, 2004; Harrison *et al.,* 2011). Coal layers outcrop along the Stenkul Fiord, literally meaning the Coal Fiord, which is part of the Eureka Sound Group coals and occurs approximately 60 km north of the Grise Fiord (Kalkreuth *et al.,* 1996). Thus, such outcropping along the watershed and river shores surrounding the Sydkap area could explain the high PAH concentrations observed in this area.

4.3. Historical trends of the PAH inputs into the sediments

Fig. 5 shows the vertical distribution (0-10 cm) of the sums of the concentrations of the 16 priority US EPA PAHs (Σ_{16}PAHs, dw) in 8 sediment cores retrieved from the CAA. The values of Σ_{16}PAHs in all sediment cores range from 8.1 to 191.1 ng g^{-1}.

In general, the inputs of PAHs during the last century seem to have remained relatively constant. The value of Σ_{16}PAHs (dw) stays within the general concentrations observed in the surface sediments of the CAA, and none of them is higher than the maximum value of 246.6 ng g^{-1} encountered in the marine sediments in this study. In regard to the surface sediments, the highest sums are found in the western CAA, especially for AMD1603-408, with a mean value of 156.2 ng g^{-1}. Very low values are obtained for AMD1902-05 (a mean value of 20.0 ng g^{-1}), a core collected near Alert (Nunavut, Canada) at the very extreme north of Ellesmere Island. This is consistent with the general trend of the decreasing PAH concentration in the sediments with increasing latitude, since remote locations are far from industrial activities, and the PAH inputs stemming from remote sources are only influenced by long-range atmospheric transport (Dong *et al.,* 2015; Balmer *et al.,* 2019). Additionally, it should be noted that in marine sediments, trends commonly tend to be less defined mainly

because of ocean perturbations (e.g., currents or ship traffic; AMAP, 2017). Therefore, variations due to worldwide fluctuations might indicate a time shift, especially because processes involving ocean currents could last years, whereas atmospheric processes are more common on a daily scale (Klungsøyr *et al.*, 2010). The PAH inputs occurring during the last century are therefore relatively stable. In sediments collected from the Barents Sea, Boitsov *et al.* (2009b) measured a 10-fold increase in the PAH concentration in marine sediments corresponding to the 1910-1940 period, while the inputs prior to 1850 remained constant. After approximately 1980, the concentration slightly decreased. This general decreasing tendency has been associated with a reduction in the worldwide PAH emissions since 1995 (Shen *et al.*, 2013). However, we do not observe this situation in our results. Additionally, Foster *et al.* (2015) studied pre-1900 and post-1900 sediments retrieved from the Baffin Bay area. The majority of their results is within a factor of 10 from those obtained for the post-1900 sediments, indicating a constant PAH concentration over time, which is consistent with our results.

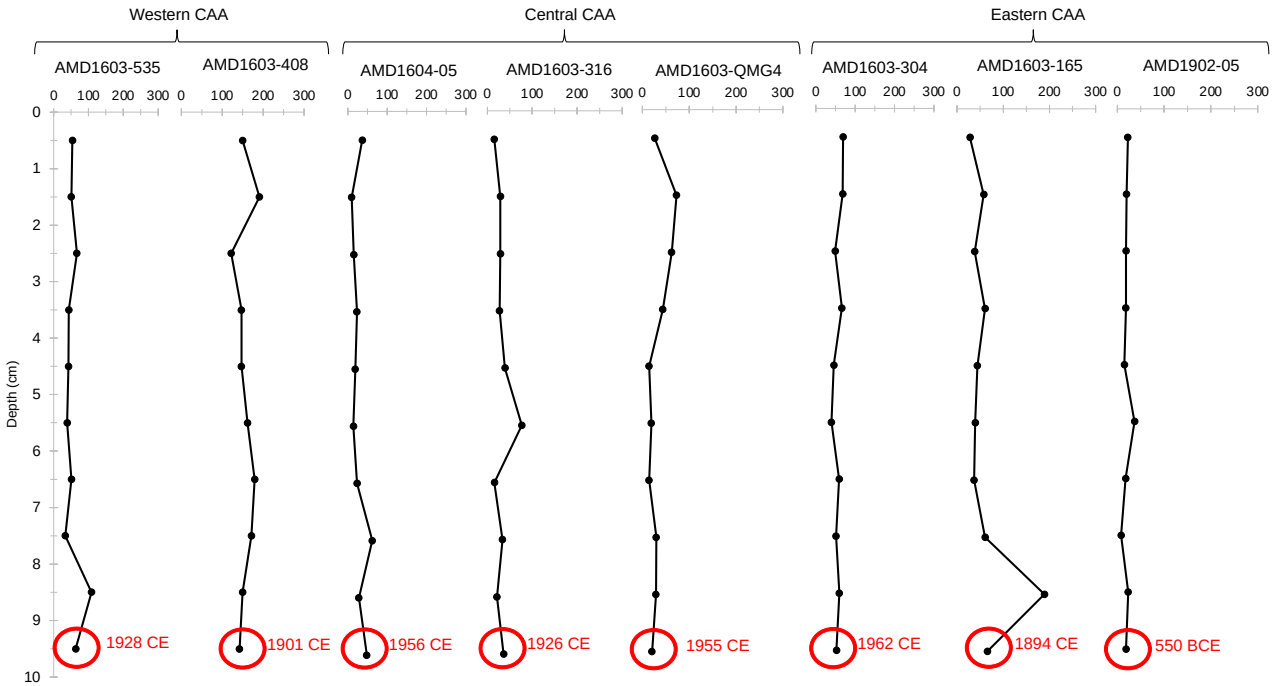

Fig. 5. Profiles of Σ_{16}PAHs (ng g^{-1} dw) in the selected box cores from western to eastern CAA. The estimated age (CE and BCE) at a core depth of 10 cm is indicated in red.

4.4. Source of the PAHs in the recent and historic sediments

4.4.1. *Diagnostic ratios*

The ratio of fluoranthene over the sum of fluoranthene and pyrene (Fla/[Fla+Pyr]) and the ratio of benz(a)anthracene over the sum of benz(a)anthracene and chrysene have been successfully applied in previous studies to determine the PAH sources in recent and preindustrial sediments (e.g., Yunker *et al.*, 2002b; Foster *et al.*, 2015). Typically, Fla/(Fla+Pyr) ratios below 0.4 are representative of petrogenic PAHs, those between 0.4 and 0.5 are representative of fossil fuel combustion and those above 0.5 are representative of biomass combustion (Yunker *et al.*, 2002b). In regard to the ratio benz(a)anthracene over the sum of benz(a)anthracene and chrysene (BaA/[BaA+Chr]), a ratio below 0.2 indicates a petrogenic source, a ratio ranging from 0.2 and 0.35 indicates a mixed source (i.e., either fossil fuel or biomass combustion) and a ratio above 0.35 indicates a pyrogenic source (Yunker *et al.*, 2002b).

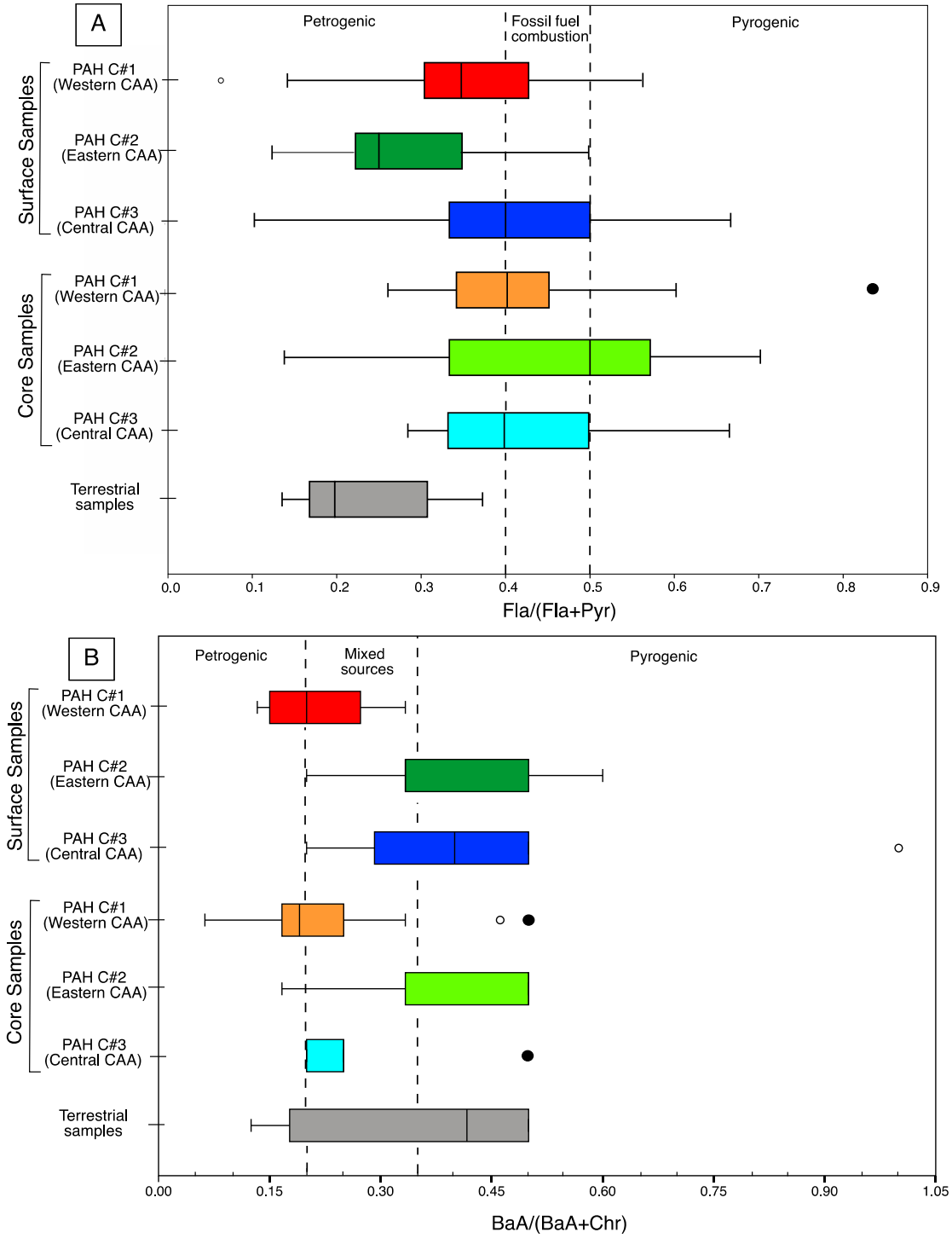

Fig. 6. Diagnostic ratios of the PAH sources: (A) ratio of fluoranthene over the sum of fluoranthene and pyrene (Fla/[Fla+Pyr]) and (B) ratio of benz(a)pyrene over the sum of benz(a)pyrene and chrysene (BaA/[BaA+Chr]) for all samples. The dashed lines indicate the ratio boundaries.

In regard to the surface samples retrieved from the western CAA, the Fla/Fla+Pyr values ranged from 0.14 to 0.56, and the BaA/(BaA+Chr) values ranged from 0.13 to 0.33, indicating a mainly petrogenic origin (Fig. 6A-B) with a small influence of mixed combustion origins. This is in agreement with the results reported for the Mackenzie River basin (Yunker *et al*., 2002a, 2011), suggesting that erosion of the organic-rich rocks of the Devonian Canol formation in the lower Mackenzie River valley contributes large amounts of petrogenic hydrocarbons to the shelf. Additionally, the hydrocarbon sources of the Mackenzie Shelf and Canada Basin sediments exhibit a strong signal originating from vascular plants and petrogenic input that is likely to overwhelm a possible combustion signal, leading to a petrogenic signal (Yunker *et al.*, 2011). In the western Arctic Ocean, Ma *et al.* (2017) also reported a mixed petrogenic and pyrogenic source for the PAHs in the surface sediments of the Chukchi Sea and Canada Basin, in line with our results. In the global Arctic Ocean, it has been reported that the natural background signature of petrogenic PAHs seemed to dominate the signal in sediments (Yunker *et al.*, 2011).

Similarly, the surface samples collected from the central CAA appeared to largely exhibit petrogenic signatures, as the Fla/(Fla+Pyr) values ranged from 0.13 to 0.50 (Fig. 6A). However, the BaA/(BaA+Chr) values ranged from 0.20 to 0.6, suggesting a mixed source/pyrogenic source. Regarding the surface samples retrieved from the eastern CAA, the Fla/(Fla+Pyr) values ranged from 0.13 to 0.67, and the BaA/(BaA+Chr) values ranged from 0.20 to 0.50, indicating a well-mixed origin from both petrogenic and pyrogenic sources (Fig. 6A-B). Thus, the central and eastern CAA exhibit a greater pyrogenic influence than the western CAA. It was previously established that the diagnostic ratios for sediments from remote areas might reflect a more pyrogenic influence because the main PAH sources are atmospheric deposition followed by sedimentation (Tsapakis *et al*., 2003; Tobiszewski and Namieśnik, 2012), which could explain our results. Ma *et al.* (2017) and Zhao *et al.* (2016) also reported that the PAHs in samples retrieved from the Arctic Ocean and the Makarov Basin originated from a mixture of petroleum and biomass combustion. However, although

diagnostic ratios are useful for discriminating the origins of PAHs, they should be interpreted with caution due to different environmental processing of the isomers during transport processes (e.g., Galarneau, 2008; Yunker *et al.*, 2002a,b, 2011). For example, degradation and/or transformation occurring during atmospheric processes and transport through the water column of the less stable fluoranthene and benz(a)anthracene might contribute to bias in old sediments (Yunker *et al.*, 2002a, 2002b, 2011). Tobiszewski and Namieśnik (2012) also suggested that the ratio of Fla/(Fla+Pyr) was more conservative than other ratios (e.g., BaA/[BaA+Ch] and anthracene over the sum of anthracene and phenanthrene; Ant/[Ant+Phe]) during atmospheric photoreactions.

Pyrogenic PAHs stemming from anthropogenic combustion have been widely detected in atmospheric samples retrieved from remote areas in the Arctic, such as Alert (Yu *et al.*, 2019). Modeling studies have shown that long-range atmospheric transport of PAHs from urban areas to remote Arctic regions occurs (Chen *et al.*, 2018). More specifically, air mass trajectory modeling performed at Alert (Nunavut, Canada) has suggested that the atmospheric PAHs in this region mainly originate from Eurasia, North Europe and North America, while East China is a minor contributor (Wang *et al.*, 2010). Hence, the main anthropogenic PAH source in the Canadian Arctic is the atmospheric deposition of PAHs stemming from worldwide hydrocarbon consumption (Klungsøyr *et al.*, 2010; Yunker *et al.*, 2011). It has also been proposed that local anthropogenic sources are actually negligible compared to deposition from remote sources (e.g., Rose *et al.*, 2004; Wang *et al.*, 2010).

In addition, forest fires are also a contributor to atmospheric pyrogenic PAHs, with an annual budget of approximately 9 tons in the Canadian Arctic, and pyrogenic PAHs have become more frequently detected in atmospheric samples since 2005 (Klungsøyr *et al.*, 2010; Yu *et al.*, 2019). Ma *et al.* (2017) found a pyrogenic influence in deep ocean sediments of the central Arctic Ocean stemming from forest fire events. These events could explain the pyrogenic signal observed in the central and eastern CAA, especially since forest fire events had increased in Canada. For example, the average annual burned area was approximately 1

million hectares in the early 1920s and reached 2 million hectares in the 2010s, with a maximum area of 2.75 million hectares in the 1990s (Wildland Fire Management Working Group, 2013). In Frobisher Bay, near Iqaluit, it appears that anthropogenic activities could locally contribute to pyrogenic PAHs in the bay (Fig. S6). The city, home to more than 7700 people, produces its electricity via imported diesel fuel (Government of Canada, 2017). In 2017, its main greenhouse gas emission sectors were the transportation, industry and electricity sectors (Government of Canada, 2017), all contributing to a pyrogenic signature. Waste burning in Iqaluit is also a common practice (Giroux, 2014), and episodic landfill fire events might contribute to a local PAH input: in 2010, a landfill fire lasted 6 weeks (Harvey, 2018), while another major fire occurred between May and September in 2014 (Weichenthal *et al.*, 2015). Finally, the petrogenic signature recorded near Sydkap Glacier confirms a coal origin (Fla/[Fla+Pyr] = 0.16) rather than an anthropogenic source, as previously reported (Fig. S6).

Regarding the core samples, they all seem to exhibit a mainly petrogenic signature combined with mixed sources: the Fla/(Fla+Pyr) values range from 0.13 to 0.88, and the BaA/(BaA+Chr) values range from 0.16 to 0.50 (Figs. 6A-B and S5). These values are consistent with the results obtained for the surface samples, except for the eastern CAA core samples, in which the pyrogenic side is more abundant. Overall, it seems that the PAH sources over time have remained relatively constant since the core sample results are consistent with the surface sample results but feature a greater pyrogenic influence. Finally, the terrestrial samples exhibit Fla/Fla+Pyr values ranging from 0.14 to 0.38, which indicate a petrogenic source, whereas the BaA/(BaA+Chr) values range from 0.12 to 0.50, indicating a relatively wide range of sources, from petrogenic to mixed/pyrogenic sources. Since only 30% (n=4) of the terrestrial samples attained a BaA/(BaA+Chr) value compared to 85% (n=11) of the samples in regard to Fla/(Fla+Pyr), this pyrogenic influence might not be representative of all the terrestrial samples. However, if it is representative of the 4 samples, it might indicate a more direct connection between atmospheric pyrogenic PAHs and soils

since the sedimentary processes do not occur and that soils are mainly influenced by atmospheric deposition (Mostert *et al.*, 2010).

Finally, the results given by the diagnostic ratios should be considered with care given the unknown effect of environmental processes occurring between the emission and deposition of the PAHs (Tobiszewski and Namieśnik, 2012). Katsoyiannis and Breivik (2014) illustrated that basic conditions, such as distance from the sources and ambient temperature, have a significant influence on the molecular ratios. Additionally, diagnostic ratios established for a certain type of sediment in urban area might not be directly applicable to remote sediments; indeed, old basin sediments in the Artic Ocean are depleted in reactive and LMW PAHs from combustion related sources, and only fluoranthene, pyrene and PAHS with molecular weights greater than 252 could provide usable source ratios (Yunker *et al.*, 2011). Hence, the contradictory results obtained in this study do not mean that they are wrong: a combination of degradation during atmospheric processes and the remote locations might explain why the Fla/(Fla+Pyr) and BaA/(BaA+Chr) values are not exactly the same (Tobiszewski and Namieśnik, 2012).

4.4.2. *Principal component analysis (PCA)*

PCA based on the Σ_{16}PAH data for all samples (surface, core and terrestrial samples) revealed that PC-1 (24% of the total variance) was positively correlated with 9,10-dimethylanthracene, 3,6-dimethylphenanthrene and pyrene, whereas PC-2 (15% of the total variance) was positively correlated with chrysene, 1-methylphenanthrene and pyrene (Fig. 7A). Finally, PC-3 (14% of the total variance) was positively correlated with 1-methylnaphthalene, 2-methylnaphthalene and acenaphthene (Fig. 7B). Parent PAHs are typically more closely associated with combustion processes, while alkylated PAHs are generally derived from petrogenic PAHs (Yunker and Macdonald, 1995; Lima *et al.*, 2005, Balmer *et al.*, 2019). Hence, each score indicated a mostly petrogenic influence. Additionally, the PC-1 and PC-3 scores were negatively correlated with at least one parent PAH composed of four rings (e.g., pyrene or chrysene). Unsubstituted PAHs containing four

582 to six rings are mainly associated with combustion sources (Laflamme and Hites, 1978).
583 Hence, PCA confirms a mainly petrogenic influence with a small pyrogenic contribution to
584 the PAHs occurring in the surface, core and terrestrial sediments within the CAA.

585 Overall, both diagnostic ratios support the predominant petrogenic nature of the
586 PAHs in the surface sediments of the CAA (Thomas and MacDonald, 2005; Yunker *et al.*,
587 2011; Foster *et al.*, 2015; Yu *et al.*, 2019). These petrogenic sources are presumably derived
588 from hydrocarbon seeps, weathering of organic-rich rocks, and coastal terrestrially derived
589 material. Strong pyrogenic influences are observed in the central and eastern CAA and are
590 likely due to forest fire events plus long-range atmospheric transport and deposition of PAHs
591 originating from distant sources. Other pyrogenic influence might occur because the remote
592 locations are mainly influenced by deposition of atmospheric pyrogenic PAHs, as previously
593 mentioned. Our results are comparable to those of previous studies pointing to petrogenic
594 sources of the PAHs in the surface sediments of the Mackenzie River/Delta, Beaufort Sea,
595 Nansen Basin, and North Baffin Bay (Yunker *et al.*, 2011, Foster *et al.*, 2015) and mixed
596 sources in the surface sediments of North Baffin Bay, Greenland Sea and north Barents Sea
597 (Yunker *et al.*, 2011; Foster *et al.*, 2015).

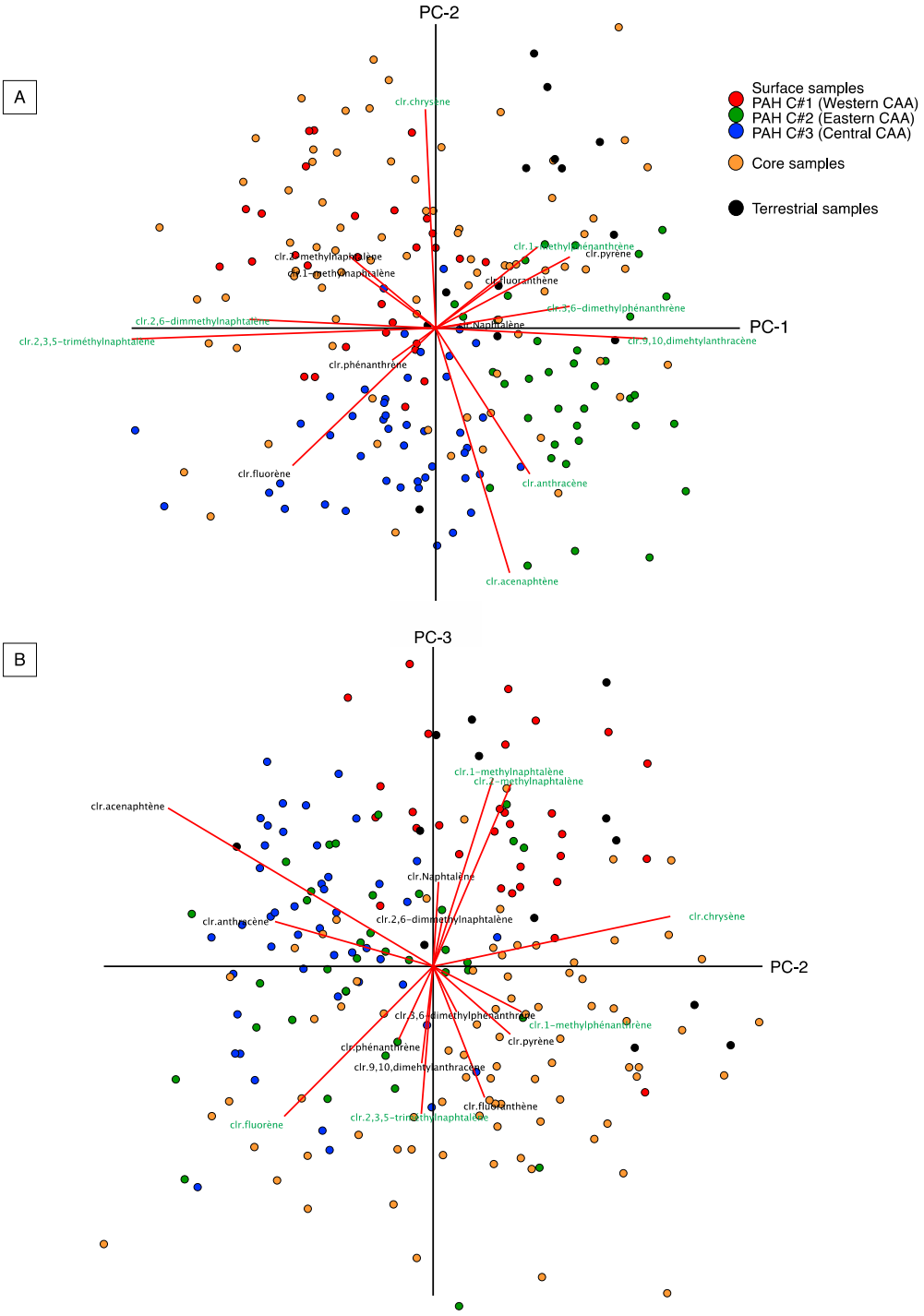

598

599 **Fig. 7**. Biplot of PC-1 versus PC-2 (A) and of PC-2 versus PC-3 (B) obtained from the log-
600 centered transformation of the PAH data of the CAA sediments. The PAHs that dominate
601 each PC score are marked in green.

602 **4.5. Risk assessment of the PAHs**

603 The potential ecological risk of the PAHs in sediments can be determined based on
604 guideline values, such as the effects range-low (ERL, the probability of adverse biological
605 effects is <10%) and effects range-median (ERM, the probability of adverse biological
606 effects is >50%) values, as proposed by Long *et al.* (1995). The PAH content ranges in the
607 CAA sediments are almost all below the ERL and ERM values (Table 3), indicating that the
608 measured PAHs pose a low ecological risk to the benthic organisms or other organisms living
609 near the sediments. Only fluorene might be an exception and would require greater attention.
610 The sample with a result of 23.7 ng g^{-1} is located in the Amundsen Gulf. This result excludes
611 the next highest value for fluorene, 15.9 ng g^{-1}, and all samples are therefore below the above
612 ERL and ERM values.

613

614 **Table 3.** Risk assessment of the PAHs in the sediments retrieved from the study area

Compound	Content range (ng g^{-1} dw)			ERL	ERM
	Surficial sediments	Terrestrial sediments	Core sediments		
Naphthalene	ND - 27.2	3.9 - 20.5	0.0 - 13.7	160	2100
2-Methtlnaphthalene	ND - 36.1	2.0 - 13.4	0.0 - 22.1	70	670
Acenaphthylene	ND - 3.0	0.0 - 2.2	0.0 - 0.3	44	640
Acenaphthene	0.0 - 9.1	0.0 - 2.2	0.0 - 5.9	16	500
Fluorene	0.0 - 23.7	0.0 - 11.2	ND - 12.1	19	540
Phenanthrene	0.0. - 63.5	0.0 - 10.1	ND - 61.2	240	1500
Anthracene	ND - 8.9	ND - 9.0	ND - 4.5	85.3	1100
Fluoranthene	0.0 - 23.7	0.0 - 40.3	0.0 - 28.4	600	5100
Pyrene	0.0 - 79.5	2.8 - 205.9	ND - 81.3	665	2600
Benz(a)anthracene	ND - 7.8	ND - 6.0	ND - 16.3	261	1600
Chrysene	2.9 - 42.2	0.0 - 30.0	ND - 22.1	384	2800
Benzo(a)pyrene	0.0 - 96.7	0.0 - 11.0	0.0 - 29.8	430	1600
Dibenz(a,h)anthracene	0.0 - 6.3	0.0 - 11.0	0.0- 3.7	63.4	260

615 ND = Not detected; ERL and ERM values from Long *et al.,* 1995.

616

617

5. Conclusions

This study provides a robust baseline record of the PAHs in surface and core marine sediments and on-land sediments retrieved from the CAA. The results of this research yield the following generalizations and conclusions:

1. The CAA is divided into 3 areas with distinct PAH compositions: (a) the western CAA, characterized by MMW (4-5 rings) to HMW (6 rings) PAHs; (b) the central CAA, characterized by LMW (2-3 rings) PAHs; and (c) the eastern CAA, characterized by MMW PAHs.

2. The sums of the concentrations of the 16 priority PAHs designated by the US EPA in both the marine and terrestrial sediments of the CAA are fairly low and comparable to other sediment levels reported for Arctic remote regions. Indeed, our results reveal Σ_{16}PAH values ranging from 7.8 to 247.7 ng g^{-1} for the total CAA, while the terrestrial sediments exhibit values ranging from 23.1 to 108.8 ng g^{-1}. Overall, regarding Σ_{16}PAHs, the different regions are classified as follows: central CAA < eastern CAA < terrestrial sediments < western CAA. Additionally, the values of Σ_{16}PAHs in the sediments are all below the ERL and ERM guidelines, except for a single sample retrieved from the Amundsen Gulf, which exhibits a fluorene content above the ERL value.

3. The inputs throughout the last century have remained relatively stable and below the maximum sum obtained for the surface sediment samples, with the Σ_{16}PAH values in the core samples ranging from 8.1 to 191.1 ng g^{-1} with a very low Σ_{16}PAH value in the northernmost core located in the Robertson Channel.

4. The diagnostic ratios of Fla/(Fla+Pyr) and BaA/(BaA+Chr), in addition to the PCA results of the PAH data, suggest that the PAHs mainly have a natural petrogenic origin, but the central and eastern CAA areas also contain PAHs originating from both fossil fuel and biomass burning, likely because of the increase in forest fire events in northern Canada in recent decades and long-range atmospheric deposition of PAHs stemming from urban areas located further south. However, diagnostic ratios should be used with care when applied to

sediments from remote locations: PAHs might undergo major environmental processes before their deposition, which could lead to bias and complications in interpreting diagnostic ratio values.

Acknowledgments

We sincerely thank the captain, crew and scientific participants of the 2016, 2017, 2018, and 2019 ArcticNet expeditions onboard CCGS Amundsen for the recovery of the sediment samples used in this study. We also thank Quentin Beauvais (UQAR-ISMER) and Steeven Ouellet (UQAR) for all their technical support and advice in the laboratory. This study was supported by ArcticNet, Québec-Océan, CREATE ArcTrain program, and the Natural Sciences and Engineering Research Council of Canada (NSERC) through Discovery Grants provided to J.-C. Montero-Serrano and the *Fonds de recherche du Québec - Nature et technologies* (FRQ-NT) MSc scholarship provided to the first author. All analytical data presented will be available electronically in the PANGAEA database (https://pangaea.de/).

CRediT authorship contribution statement

Anne Corminboeuf: investigation, writing – original draft.

Jean-Carlos Montero-Serrano: conceptualization, resources, writing – review and editing, funding acquisition.

Richard St-Louis: conceptualization, resources, writing – review and editing.

References

Alkire, M.B., Jacobson, A.B., Lehn, G.O., Macdonald, R.W., Rossi, M.W. 2017. On the geochemical heterogeneity of rivers draining into the straits and channels of the Canadian Arctic Archipelago. Journal of Geophysical Research: Biogeosciences, 122(10), 2527-2547.

Aitchison, J.1986. The statistical analysis of compositional data. Monographs on statistics and applied Probability: Chapman & Hall, London (Reprinted in 2003 with additional material by Blackburn Press), 416 p.

Aitchison, J. 1990. Relative variation diagrams for describing patterns of compositional variability. Mathematical Geology, 22(4), 487–511.

AMAP, 2017. AMAP Assessment 2016: Chemical of emerging Arctic concern. Arctic Monitoring and Assessment Program (AMAP), Oslo, Norway, (16) 353.

Appleby, P. G., Oldfieldz, F. 1983. The assessment of 210Pb data from sites with varying sediment accumulation rates. Hydrobiologia, 103(1), 29-35.

Askenov, Y., Popova, E.E., Yool, A., George Nurser, A.J., Williams, T.D., Bertino, L., Bergh, J. 2017. On the future navigability of Arctic sea routes: High-resolution projections of the Arctic Ocean and sea ice. Marine Policy 75, 300–317.

Balmer, J.E., Hung, H., Yu, Y., Letcher, R.J., Muir, D.C.G. 2019. Sources and environmental fate of pyrogenic polycyclic aromatic hydrocarbons (PAHs) in the Arctic. Emerging Contaminants, 5, 128-142.

Blasco, S., Bennett, R., Kostylev, V., Campbell, P., Shearer, J., Conlan, K. 2006. Seabed topography, geological structure and evolution of the sea-ice regime on the Beaufort Shelf at the western entrance to the Northwest Passage: CCGS Nahidik Research. The Canadian Geomorphology Research Group, 3rd Annual ArcticNet Scientific meeting. December 12-15, 2006. Victoria, British-Colombia.

Boitsov, S., Jensen, H.K.B., Klungsøyr, J. 2009a. Geographical variations in hydrocarbon levels in sediments from the Western Barents Sea. Norwegian Journal of Geology, 89, 91-100.

Boitsov, S., Jensen, H.K.B., Klungsøyr, J. 2009b. Natural background and anthropogenic inputs of polycyclic aromatic hydrocarbons (PAH) in sediments of the south-western Barents Sea. Marine Environmental Research, 68, 236-245.

Borcard, D., Gillet, F., Legendre, P. 2011. Numerical ecology with R, Springer, New York.

Charrad, M., Ghazzali, N., Boiteau, V., Niknafs, A. 2014. Nbclust: an R package for determining the relevant number of clusters in a data set. Journal of Statistical Software, 61, 1–36.

Chen, F., Lin, Y., Cai, M., Zhang, J., Zhang, Y., Kuang, W., Liu, L., Huang, P., Ke, H. 2018. Occurrence and risk assessment of PAHs in surface sediments from Western Arctic and Subarctic Ocean. International Journal of Environmental Research and Public Health, 15, 734.

Chiou, C.T., McGroddy, S.E., Kile, D.E. 1998. Partition characteristics of polycyclic aromatic hydrocarbons on soils and sediments. Environmental Science & Techonology, 32 (2) 264-269.

Choi, M., Kim., Y.-J., Lee, I.-S., Choi, H.-G. 2014. Development of a one-step integrated pressurized liquid extraction and cleanup method for determining polycyclic aromatic hydrocarbons in marine sediments. Journal of Chromatography A, 1340, 8-14.

Comas, M., Thió-Henestrosa, S. 2011. CoDaPack v2.02.21: a stand-alone, multi-platform compositional software. CoDaWork'11: 4th International Workshop on Compositional Data Analysis 1-10.

Darby, D.A. 2003. Sources of sediment found in sea ice from the western Arctic Ocean, new insights into processes of entrainment and drift patterns. Journal of Geophysical Research 108, 1–10.

Darby, D.A., Nyers, W.B., Jakobsson, M. and Rigor, I. (2011). Modern dirty sea ice characteristics and sources: The role of anchor ice. Journal of Geophysical Research, 116,18 pp.

Dong, C., Bai, X., Sheng, H., Jiao, L., Zhou, H., Shao, Z. 2015. Distribution of PAHs and the PAH-degrading bacteria in the deep-sea sediments of the high-latitude Arctic Ocean. Biogesciences, 12, 2163-2177.

Dowdeswell, J. A., Hogan, K. A., Arnold, N. S., Mugford, R. I., Wells, M., Hirst, J. P. P., Decalf, C. 2015. Sediment-rich meltwater plumes and ice-proximal fans at the margins of modern and ancient tidewater glaciers: Observations and modelling. Sedimentology, 62(6), 1665–1692.

Foster, K.L., Stern, G.A., Carrie, J., Bailey, J.N.-L., Outridge, P.M., Sanei, H., Macdonald, R.W. 2015. Spatial, temporal, and source variations of hydrocarbons in marine sediments from Baffin Bay, Eastern Canadian Arctic. Science of the Total Environment, 506-507, 430-443.

Galarneau, E. 2008. Sources specificity and atmospheric processing of airborne PAHs: Implication for source apportionment. Atmospheric Environment, 42(35), 8139-8149.

741 Giroux, L. 2014. State of waste management in Canada. Report prepared for the Canadian
742 Council of Ministers of Environment (CCME). [PDF]:
743 https://www.ccme.ca/files/Resources/waste/wst_mgmt/State_Waste_Mgmt_in_Canada
744 %20April%202015%20revised.pdf

745 Government of Canada. 2017. Provincial and territorial energy profiles – Nunavut. [URL]:
746 https://www.cer-rec.gc.ca/nrg/ntgrtd/mrkt/nrgsstmprfls/nu-eng.html

747 Gschwend, P.M., Hites, R. 1981. Fluxes of polycyclic aromatic hydrocarbons to marine and
748 lacustrine sediments in the northeastern United States. Geochimica et Cosmochimica
749 Acta, 45, 2359-2367.

750 Haritash, A.K., Kaushik, C.P. 2009. Biodegradation aspects of polycyclic aromatic
751 hydrocarbons (PAHs): A review. Journal of Hazardous Materials, 169, 1-15.

752 Harris, P.T. 2012. Seafloor geomorphology – Coast, shelf, and abyss. Seafloor
753 geomorphology as benthic habitat, GeoHAB atlas of seafloor geomorphic features and
754 benthic habitats, 109-155.
755
756 Harrison, J.C., St-Onge, M.R., Petrov, O.V., Strelnikov, S.I., Lopatin, B.G., Wilson, F.H.,
757 Tella, S., Paul, D., Lynds, T., Shokalsky, S.P., Hults, C.K., Bergman, S., Jepsen, H.F.,
758 Solli, A. 2011. Geological map of the Arctic, Geological Survey of Canada, Open
759 Access: https://doi.org/10.4095/287868.
760
761 Harvey, M. 2018. Discussions sur le futur dépotoir de la ville d'Iqaluit, dans le nord canadien.
762 Radio-Canada International, [URL]: https://www.rcinet.ca/regard-sur-
763 arctique/2018/11/19/depotoir-iqaluit-dechets-enfouissement-nunavut-enfouissement-
764 pollution/

765 Hiscott, R. N., Aksu, A. E., Nielsen, O. B. 1989. Provenance and dispersal patterns, Pliocene-
766 Pleistocene section at site 645, Baffin Bay. Proceedings of the Ocean Drilling Program,
767 Scientific Results, 105, 31-52.

768 IARC, 1987. IARC Monographs on the Evaluation of the Carcinogenic Risk of Chemicals
769 to Humans. Overall Evaluations of Carcinogenicity: An Updating of the IARC
770 Monographs Vol. 1 to 42, Supplement 7. International Agency for Research on Cancer,
771 WHO, Lyon, France.

772 Janicki, E. 2001. A brief history of hydrocarbons exploration in the North-west Territories.
773 A publication of the C.S. Lord Northern Geosciences Center, North-west Territories
774 Geosciences Center.

775 Jennings, A.E., Sheldon, C., Cronin, T.M., Francus, P., Stoner, J., Andrews, J. 2011. The
776 Holocene history of Nares Strait: Transition from glacial bay to Arctic-Atlantic
777 throughflow. Oceanography, 24(3), 26-41.

778 Jiao, L.P., Zheng, G.J., Minh, T.B., Richardson, B., Chen, L.Q., Zhang, Y.H., Yeung, L.W.,
779 Lam, J.C.W., Yang, X.L., Lam, P.K.S., Wong, M.H. 2009. Persistent toxic substances
780 in remote lake and coastal sediments from Svalbard, Norwegian Arctic: levels, sources
781 and fluxes. Environmental Pollution, 157, 1342-1351.

782 Jörrundsdóttir, H.O., Jensen, S., Hylland, K., Holth, T.F., Gunnlaugsdóttir, H., Svavarsson,
783 J., Ólafsdóttir, El-Taliawy, H., Rigét, F., Strand, J., Nyberg, E., Bignert, A., Hoydal,
784 K.S., Pálmar Halldórsson, H. 2014. Pristine Arctic: Background mapping of PAHs, PAH
785 metabolites and inorganic trace elements in the North-Atlantic Arctic and sub-Arctic
786 coastal environment. Science of the Total Environment, 493 (2014) 719-728.

787 Kalkreuth, W.D., Riediger, C.L., McIntyre, D.J., Richardson, R.J.H., Fowler, M.G.,
788 Marchioni, D. 1996. Petrological, palynological and geochemical characteristics of
789 EurekaSound Group coals (Stenkul Fiord, southern Ellesmere Island, Arctic Canada).
790 International Journal of Coal Geology, 30, 151-182.

791 Kalkreuth, W.D. 2004. Coal facies studies in Canada, International Journal of Coal Geology,
792 58, 23-30.

793 Katsoyiannis, A., Breivik, K. 2014. Model-based evaluation of the use of polycyclic aromatic
794 hydrocarbons molecular diagnostic ratios as source identification tool. Environmental
795 Pollution, 184, 488-494.

796 Kaufman, L., Rousseeuw, P.J. 2009. Finding groups in data: an introduction to cluster
797 analysis, John Wiley & Sons.

798 Keith, L.H. 2014. The Source of U.S. EPA's sixteen PAH priority pollutants. Polycyclic
799 Aromatic Compounds, 35, 147-160.

800 Klungsøyr, S.L., Dahle, S., Thomas, D.J. 2010. Sources, inputs and concentrations of
801 petroleum hydrocarbons, polycyclic aromatic hydrocarbons, and other contaminants
802 related to oil and gas activities in the Arctic. In: AMAP Assessment 2007: Oil and gas
803 activities in the Arctic – Effects and Potentiel Effects. Volume 2, chapter 4. Arctic
804 Monitoring and Assessment Programme (AMAP).

805 Lai, S.YJ., Gerber, T.P., Amblas, D. 2016. An experimental approach to submarine canyon
806 evolution. Geophysical Research Letters, 43 (6), 2741-2747.
807
808 Laflamme, R.E., Hites, R.A. 1978. The global distribution of polycyclic aromatic
809 hydrocarbons in recent sediments. Geochimica et Cosmochimica Acta, 41, 289-303.

810 Lammel, G., Sehili, A. M., Bond, T. C., Feichter, J., Grassl, H. 2009. Gas/particle
811 partitioning and global distribution of polycyclic aromatic hydrocarbons – A modelling
812 approach. Chemosphere, 76(1), 98–106.

Lasserre, F. 2010. Vers l'ouverture d'un Passage du Nord-Ouest stratégique ? Entre les États-Unis et le Canada. Outre-Terre, 25-26 (2), 437-452.

Letaïef, S. 2019. Les processus sédimentaires durant le Petit âge glaciaire et l'actuel dans l'Archipel arctique canadien. Mémoire. Rimouski, Université du Québec à Rimouski, Institut des sciences de la mer de Rimouski (ISMER), 96 p. http://semaphore.uqar.ca/id/eprint/1500/

Levy, E.M. 1978. Visual and chemical evidence for a natural seep at Scott Inlet, Baffin Island, District of Franklin. Geological Survey of Canada, pp. 21-26. Current Research Paper: 78-1B.

Lima, A.L., Farrington, J.W., Reddy, C.M. 2005. Combustion-derived polycyclic aromatic hydrocarbons in the environment – A review. Environmental Forensics, 6, 109-131.

Long, E.R., MacDonal, D.D., Smith, S.L., Calder, F.D. 1995. Incidence of adverse biological effects within ranges of chemical concentrations in marine and estuarine sediments. Environmental Management, 19(1), 81-97.

Ma, Y., Halsall, C.J., Xie, Z., Koetke, D., Mi, W., Ebinghaus, R., Gao, G. 2017. Polycyclic aromatic hydrocarbons in ocean sediments from the North Pacific to the Arctic Ocean. Environmental Pollution, 227, 498-504.

Madaj, L. 2016. Holocene organic carbon and carbonate records from the Northeast Baffin Bay: preliminary age model and paleoenvironmental significance, Msc. Thesis, Department of Earth Sciences, University of Gothenburg, Gothenburg, Sewden, 48p.

Maechler, M., Rousseeuw, P., Struyf, A., Hubert, M., Studer, M., Roudier, P. 2019. Finding Groups in Data: Cluster Analysis Extended Rousseeuw et al. R package. [Available at https://cran.r-project.org/web/packages/cluster/]

Melling, H. 2002. Sea ice of the Northern Canadian Arctic Archipelago. Journal of Geophysical Research, 107 (C11) 3181.

Michel, C., Ingram, R.G., Harris, L.R. 2006. Variability in oceanographic and ecological processes in the Canadian Arctic Archipelago. Progress in oceanography, 71, 379-401.

Montero-Serrano, J. C., Palarea-Albaladejo, J., Martin-Fernandez, J.-A., Martinez-Santana, M., Gutierrez-Martin, J. V. 2010. Sedimentary chemofacies characterization by means of multivariate analysis. Sedimentary Geology, 228, 218–228, doi:10.1016/j.sedgeo.2010.04.013.

Montero-Serrano, J. C., Rioux P., Aebischer, S. 2016. Natural climate and oceanographic variability in the western Canadian Arctic Ocean since the last deglaciation. ArcticNet Leg 3a Cruise Report - CCGS Amundsen (25 August to 17 September 2016).

Montero-Serrano, J.-C., Furze, M. Zindorf, M., Pieńkowski, A. 2017. The marine sedimentary record of paleoclimate, paleoceanography, and deglacial history in the eastern Canadian Arctic Archipelago and Northern and Eastern Baffin Bay. ArcticNet Leg 2b Cruise Report - CCGS Amundsen (13 July to 17 August 2017).

Montero-Serrano, J.-C., Brossard, J., Corminboeuf, A. 2018. Collecting sedimentary sequences for paleoclimate, paleoceanographic and environmental studies in the eastern Canadian Arctic Archipelago and Baffin Bay. ArcticNet Leg 3 Cruise Report - CCGS Amundsen (16 August to 9 September 2018).

Montero-Serrano, J.-C., Brossard, J., Corminboeuf, A. 2019. Collecting sedimentary sequences and plankton samples in the continental margins from the eastern Canadian Arctic Archipelago. ArcticNet Leg 2b Cruise Report – CCGS Amundsen (25 July to 15 August 2019).

Morillo, E., Romero, A.S., Madrid, L., Villaverde, J., Maqueda, C. 2008. Characterization and sources of PAHs and potentially toxic metals in urban environments of Sevilla (Southern Spain). Water, Air and Soil Pollution, 187, 41–51.

Mostert, M.M.R., Ayoko, G.A., Kokot, S.. 2010. Application of chemometrics to analysis of soil pollutants. Trends in Analytical Chemistry, 29, 430-435.

Oblinger Childress, C.J., Foreman, W.T., Connor, B.F., Maloney, T.J. 1999. New reporting procedures based on long-term method detection levels and some considerations for interpretation of water-quality data provided by the U.S. Geological Survey National Water Quality Laboratory. US Geological Survey, open-file report 99-193.

Ó Cofaigh, C., Taylor, J., Dowdeswell, J.A., Pudsey, C.J. 2003. Palaeo-ice streams, trough mouth fans and high-latitude continental slope sedimentation. Boreas, 32, 37–55.

Palarea-Albaladejo J., Martin-Fernandez J.A. 2015. zCompositions — R package for multivariate imputation of left-censored data under a compositional approach. Chemometrics and Intelligence Laboratory Systems 143, 85-96.

Pampanin, D.M., Sydnes, M.O. 2017. Petrogenic polycyclic aromatic hydrocarbons in the aquatic environment: analysis, synthesis, toxicity and environmental impact**.** DOI:10.2174/97816810842751170101

Pelletier, E., Desbiens, I., Sargian, P., Côté, N., Curtosi, A., St-Louis, R. 2008. Présence des hydrocarbures aromatiques polycycliques (HAP) dans les compartiments biotiques et abiotiques de la rivière et du fjord du Saguenay. Revue des sciences de l'eau, 22(2), 235-251.

884 Rapinski, M., Cuerrier, A., Harris, C., Elders of Ivujivik, Elders of Kangiqsujuaq, Lemire,
885 M. 2018. Inuit perception of marine organisms: from folk classification to food harvest.
886 Journal of Ethnobiology, 38(3), 333-355.
887
888 R Core Team. 2020.. R: A language and environment for statistical computing. R Foundation
889 for Statistical Computing, Vienna, Austria. [Available at https://www.R-project.org/]

890 Reimnitz, E., Clayton, J.R., Kempema, E.W., Payne, J.R., Weber, W.S. 1993. Interaction of
891 rising frazil with suspended particles: tank experiments with applications to nature. Cold
892 Regions Science and Technology 21, 117–135. doi:http://dx.doi.org/10.1016/0165-
893 232X(93)90002-P

894 Ricketts, B.D., Embry, A.F. 1984. Summary of the geology and resource potential of coal
895 deposits in the Canadian Arctic Archipelago, Bulletin of Canadian Petroleum Geology,
896 32(4), 359-371.

897 Rose, N.L., Rose, C.L., Boyle, J.F., Appleby, P.G. 2004. Lake-sediment evidence for local
898 and remote sources of atmospherically deposited pollutants on Svalbard. Journal of
899 Paleolimnology, 31, 499-513.

900 Roslund, M.I., Grönroos, M., Rantalainen, A.-L., Jumpponen, A., Romantschuk, M.,
901 Parajuli, A., Hyöty, H., Laitinen, O., Sinkkonen, A. 2018. Half-lives of PAHs and
902 temporal microbiota changes in commonly used urban landscaping materials. PeerJ DOI
903 10.7717/peerj.4508

904 Schlitzer, R. 2015. Ocean Data View.

905 Sericano, J.L., Brooks, J.M., Champ, M.A., Kennicutt, M.C., Makeyev, V.V. 2001. Trace
906 contaminant concentrations in the Kara Sea and its adjacent rivers, Russia. Marine
907 Pollution Bulletin, 42, 1017-1030.

908 Shen, H., Huang, Y., Wang, R., Zhu, D., Li, W., Guofeng, S., Wang, B., Zhang, Y., Chen,
909 Y., Lu, Y., Chen, H., Li, T., Sun, K., Li, B., Liu, W., Liu, J., Tao, S. 2013. Global
910 Atmospheric Emissions of Polycyclic Aromatic Hydrocarbons from 1960 to 2008 and

911 Smith, L.C., Stephenson, S.R. 2013. New trans-Arctic shipping routes navigable by
912 midcentury. Proceedings of the National Academy of Sciences of the United States of
913 America, 110 (13) E191-E1195.

914 Sofowote U.M., Hung H., Rastogi A.K., Westgate J.N., Deluca P.F., Su Y., McCarry B.E.
915 2011. Assessing the long-range transport of PAH to a sub-arctic site using positive
916 matrix factorization and potential source contribution function. Atmospheric
917 Environment, 45 (4) 967-976.

Stark, A., Abrajano, T.Jr., Hellou, J., Metcalf-Smith., J.L. 2003. Molecular and isotopic characterization of polycyclic aromatic hydrocarbons distribution and sources at the international segment of the St. Lawrence River. Organic Geochemistry, 34, 225-237.

Stein, R. 1991. Organic carbon accumulation in Baffin Bay and paleoenvironment in high northern latitudes during the past 20 m.y. Geology, 19(4), 356-359.

Stein, R. 2008. Arctic Ocean Sediments: Processes, proxies and paleoenvironment. Elsevier, Developments in Marine Geology, vol.2, 591p.

Thomas, D.J. 1979. Seabed releases of gas around the Tingmiark K-91 wellsite in the southern Beaufort Sea. Dome Petroleum Ltd. Calgary, Alberta.

Thomas, D.J., Macdonald, R.W. 2005. A petroleum hydrocarbon budget for the Arctic. Presentation at the AMAP International Symposium on Oil and Gas Activities in the Arctic, pp. xxxiv. St. Petersburg, 13-15 September 2005.

Tobiszewski, M., Namieśnik, J. 2012. PAH diagnostic ratio for the identification of pollution emission sources. Environmental Pollution, 162, 110-119.

Tsapakis, M., Stephanou, E.G., Karakassis, I. 2003. Evaluation of atmospheric transport as a nonpoint source of polycyclic aromatic hydrocarbons in marine sediments of the Eastern Mediterranean. Marine Chemistry, 80, 283-298.

Van den Boogaart, K. G., Tolosana-Delgado, R. 2008. “Compositions”: a unified R package to analyze compositional data. Computers & Geosciences, 34(4), 320-338.

von Eynatten, H., Barceló-Vidal, C., Pawlowsky-Glahn, V. 2003. Sandstone composition and discrimination: A statistical evaluation of different analytical methods: Journal of Sedimentary Research, 73(1), 47-57.

Xue, W., D. Warshawsky. 2005. Metabolic activation of polycyclic and heterocyclic aromatic hydrocarbons and DNA damage: a review. Toxicology and Applied Pharmacology, 206:73-93.

Yanik, P.J., O'Donnell, T.H., Macko, S.A., Qian, Y., Kennicutt II, M.C. 2003.The isotopic compositions of selected crude oil PAHs during biodegradation. Organic Geochemistry, 34, 291–304.

Yu, Y., Katsoyiannis, A., Bohlin-Nizzetto, P., Brorström-Lundén, E., Ma, J., Zhao, Y., Wu, Z., Tych, W., Mindham, D., Sverko, E., Barresi, E., Dryfhout-Clark, H., Fellin, P., Hung, H. 2019. Polycyclic aromatic hydrocarbons not declining in Arctic air despite global emission reduction. Environmental Science & Technology, 53, 2375-2382.

Yunker, M.B., Macdonald, R.W., Fowler, B.R., Cretney, W.J., Dallimore, S.R., McLaughlin, F.A. 1991. Geochemistry and fluxes of hydrocarbons to the Beaufort Sea Shelf: A multivariate comparison of fluvial inputs and coastal erosion of peat using principal component analysis. Geochimica et Cosmochimica Acta, 55, 255-273.

Yunker, M.B., Macdonald, R.W. 1995. Composition and origins of polycyclic aromatic hydrocarbons in the Mackenzie River and on the Beaufort Sea shelf. Arctic, 48(2), 118-129.

Yunker, M.B., Snowdon, L.R., Macdonald, R.W., Smith, J.N., Fowler, M.G., Skibo, D.N., Mclaughlin, F.A., Danyushevskaya, A.I., Petrova, V.I., Ivanov, G.I. 1996. Polycyclic aromatic hydrocarbons composition and potential sources for sediment samples from the Beaufort and Barents Sea. Environmental Science & Technology, 30(4), 1310-1320.

Yunker, M.B., Backus, S.M., Graf Pannatier, E., Jeffries, D.S., Macdonald, R.W. 2002a. Sources and significance of alkane and PAH hydrocarbons in Canadian arctic rivers. Estuarine, Coastal and Shelf Science, 55, 1–31.

Yunker, M.B., Macdonald, R.W., Vingarzan, R., Mitchell, R.H., Goyette, D., Sylvestre, S. 2002b. PAHs in the Fraser River basin: a critical appraisal of PAH ratios as indicators of PAH source and composition. Organic Geochemistry, 33, 489-515.

Yunker, M.B., Macdonald, R.W., Snowdon, L.R., Fowler, B.R. 2011. Alkane and PAH biomarkers as tracers of terrigenous organic carbon in Arctic Ocean sediments. Organic Geochemistry, 42, 1109-1146.

Wagner, A., Lohmann, G., Prange, M. 2011. Arctic river discharge trends since 7ka BP. Global and Planetary Change, 79 (1) 48-60.

Walsh, F.B. 2006. The Kopanoar mud volcano on the Mackenzie Shelf, Beaufort Sea: implications for methane release on arctic shelves. Atlantic Geology, 42, 120-121.

Wang, Z., Chen, J., Yang, P., Qiao, X., Tian, F. 2007. Polycyclic aromatic hydrocarbons in Dalian soils: distribution and toxicity assessment. Journal of Environmental Monitoring, 9, 199-204.

Wang, R., Shu T., Wang B., Yu Y., Chang L., Zhang Y.X., Jing H., Ma J.M., Hung, H. 2010. Sources and pathways of polycyclic aromatic hydrocarbons transported to alert, the Canadian High Arctic. Environmental Science and Technology, 44, 1017-1022.

Weichenthal, S., Van Rikswijk, D., Kulka, R., You, H., Van Ryswyk, K., Willey, J., Dugandzic, R., Sutcliffe, R., Moulton, J., Baike, M., White, L., Charland, J.-P., Jessiman, B. 2015. The impact of a landfill fire on ambient air quality in the north: A case study in Iqaluit, Canada. Environmental Research, 142, 46-50.

Wildland Fire Management and Working Group. 2013. Evaluating past, current and future forest fire loads in Canada. Canadian Council of Forests Ministers, [PDF]: https://www.ccfm.org/pdf/2%20Fire%20Load%20Trends.pdf

Zaborska, A., Carroll, J., Pazdro K., Pempkowiak, J. 2011. Spatio-temporal patterns of PAHs, PCBs and HCB in sediments of the western Barents Sea. Oceanologia, 53, 1005-1026.

Zhang, Y., Tao, S. 2009. Global atmospheric emission inventory of polycyclic aromatic hydrocarbons (PAHs) for 2004. Atmospheric Environment, 43, 812-819.

Zhao, W., Wang., W., Liu, Y., Dong, L., Jiao, L., Hu, L., Fan, D. 2016. Distribution and sources of polycyclic aromatic hydrocarbons in surface sediments from the Bering Sea and western Arctic Ocean. Marine Pollution Bulletin, 104, 379-385.

Supplementary material

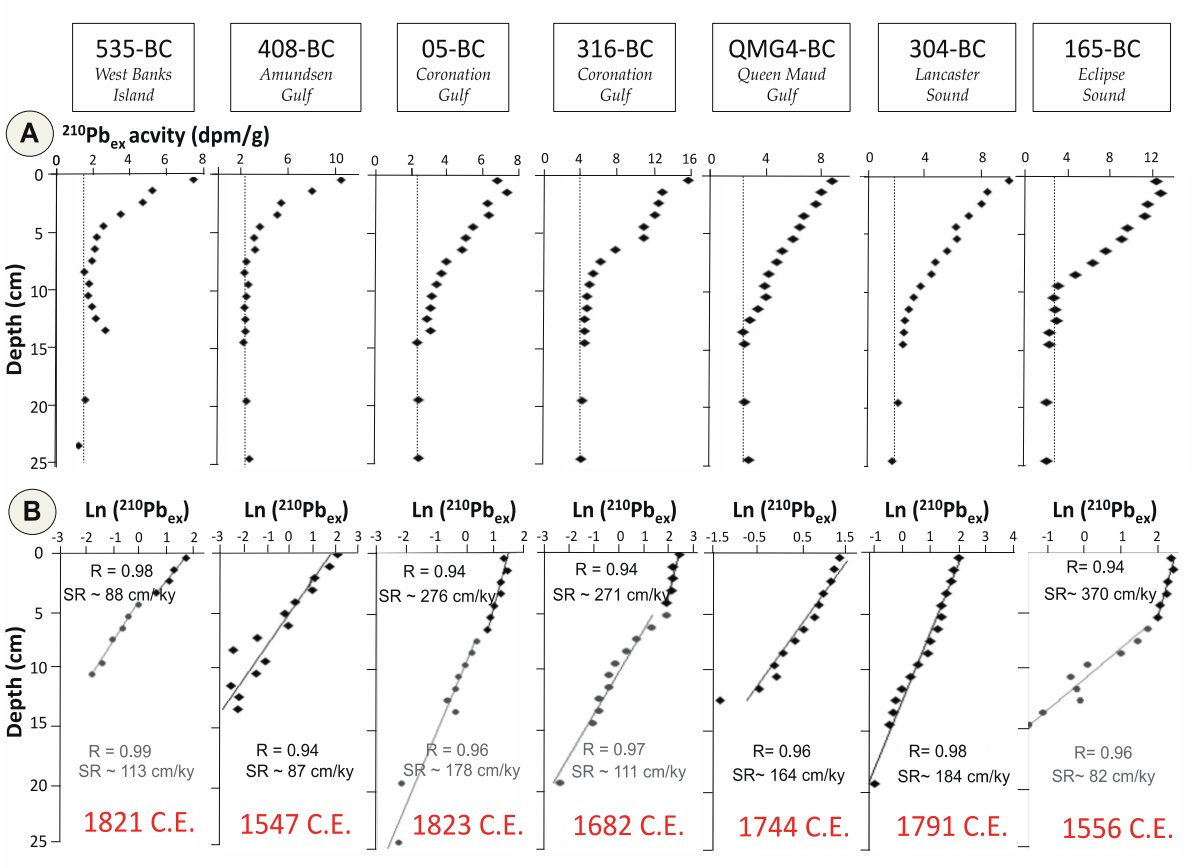

Fig. S1. ^{210}Pb chronology of the 8 box cores retrieved from the CAA studied here. The sedimentation rate used to calculate the basal age of each sediment core is also shown (Letaïef, 2019).

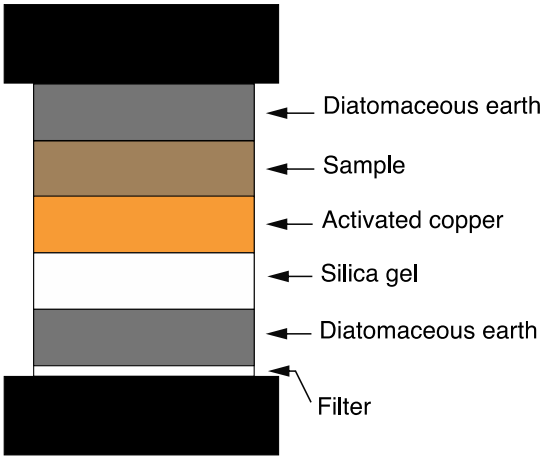

Fig. S2. Packing of the extraction cell (adapted from Choi *et al.*, 2014).

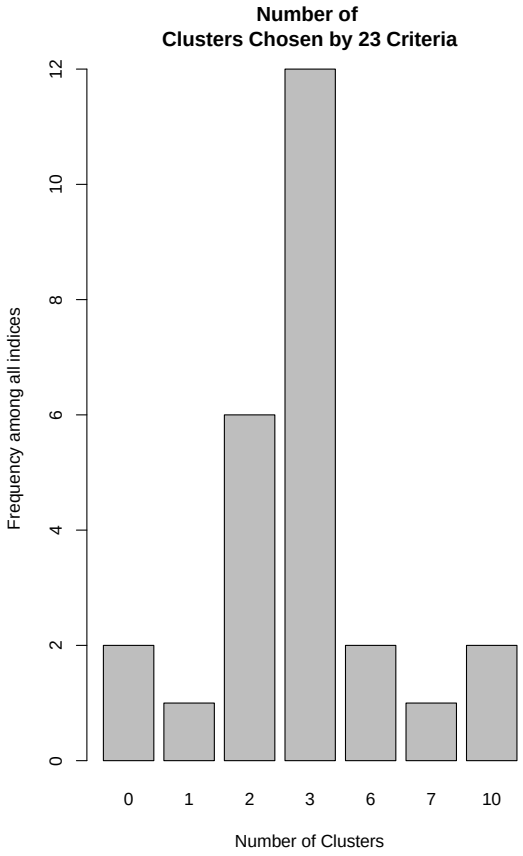

Fig. S3. NbClust result showing that the optimal number of clusters is 3.

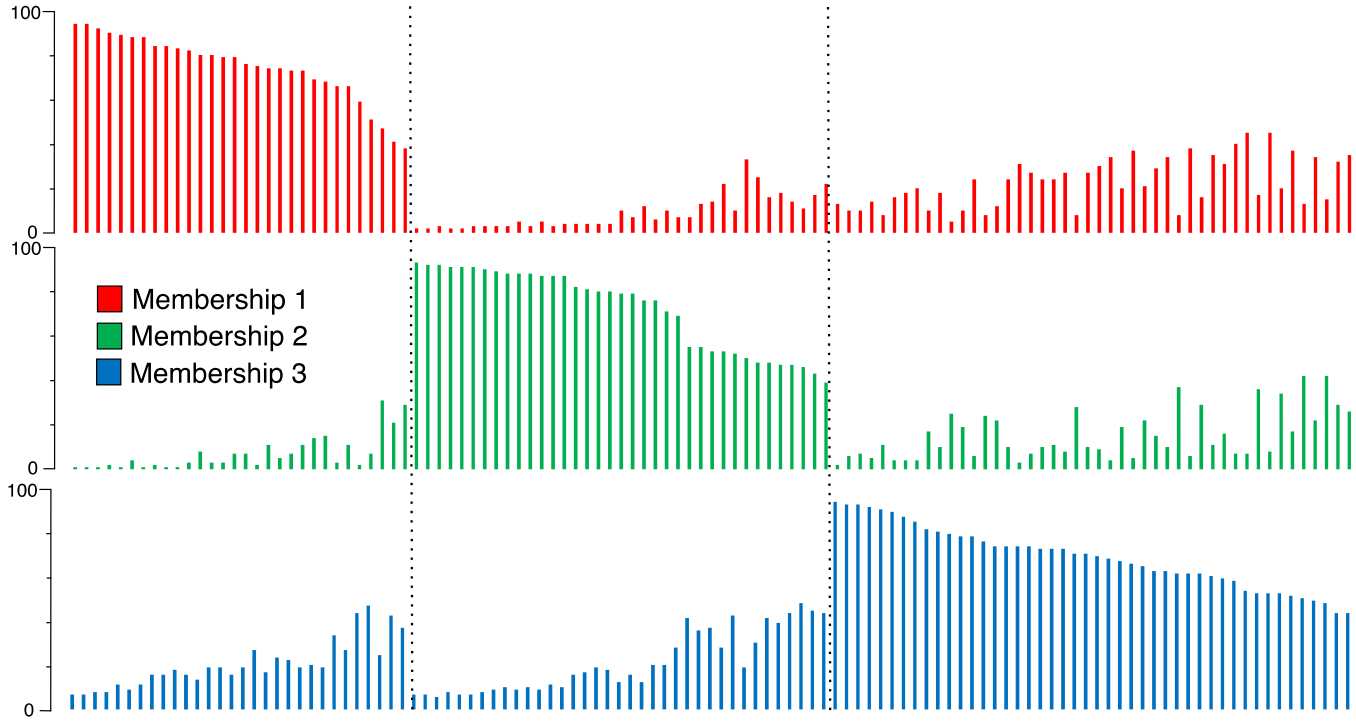

Fig. S4. Percent of samples associated with the three clusters determined in this study. The plot indicates that most of the surface samples were correctly classified, whereas 1 sample from cluster 1, 6 samples from cluster 2 and 2 samples from cluster 3 might be incorrectly classified. This is likely due to their PAH assemblages and sources.

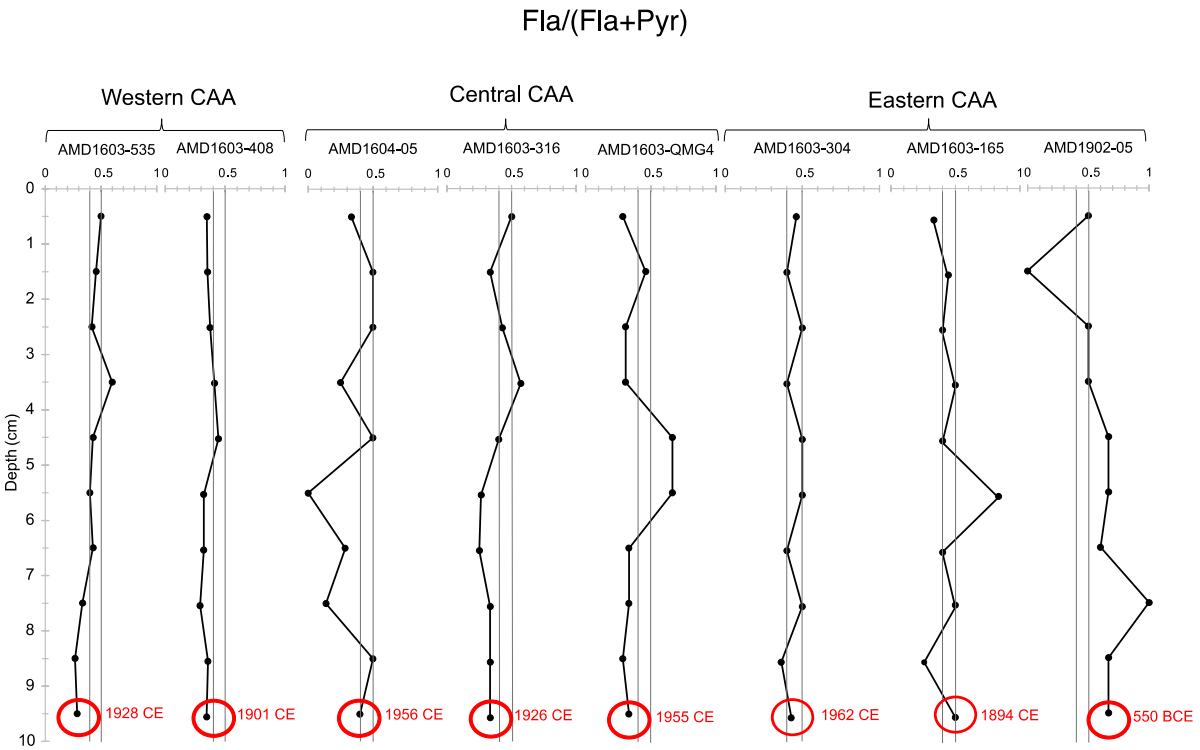

Fig. S5. Ratio of fluoranthene over the sum of fluoranthene and pyrene (Fla/[Fla+Pyr]) in the historical sediments. The solid lines indicate the ratio boundaries of 0.4 and 0.5. Red indicates the calculated age (CE or BCE) at 10 cm of the core.

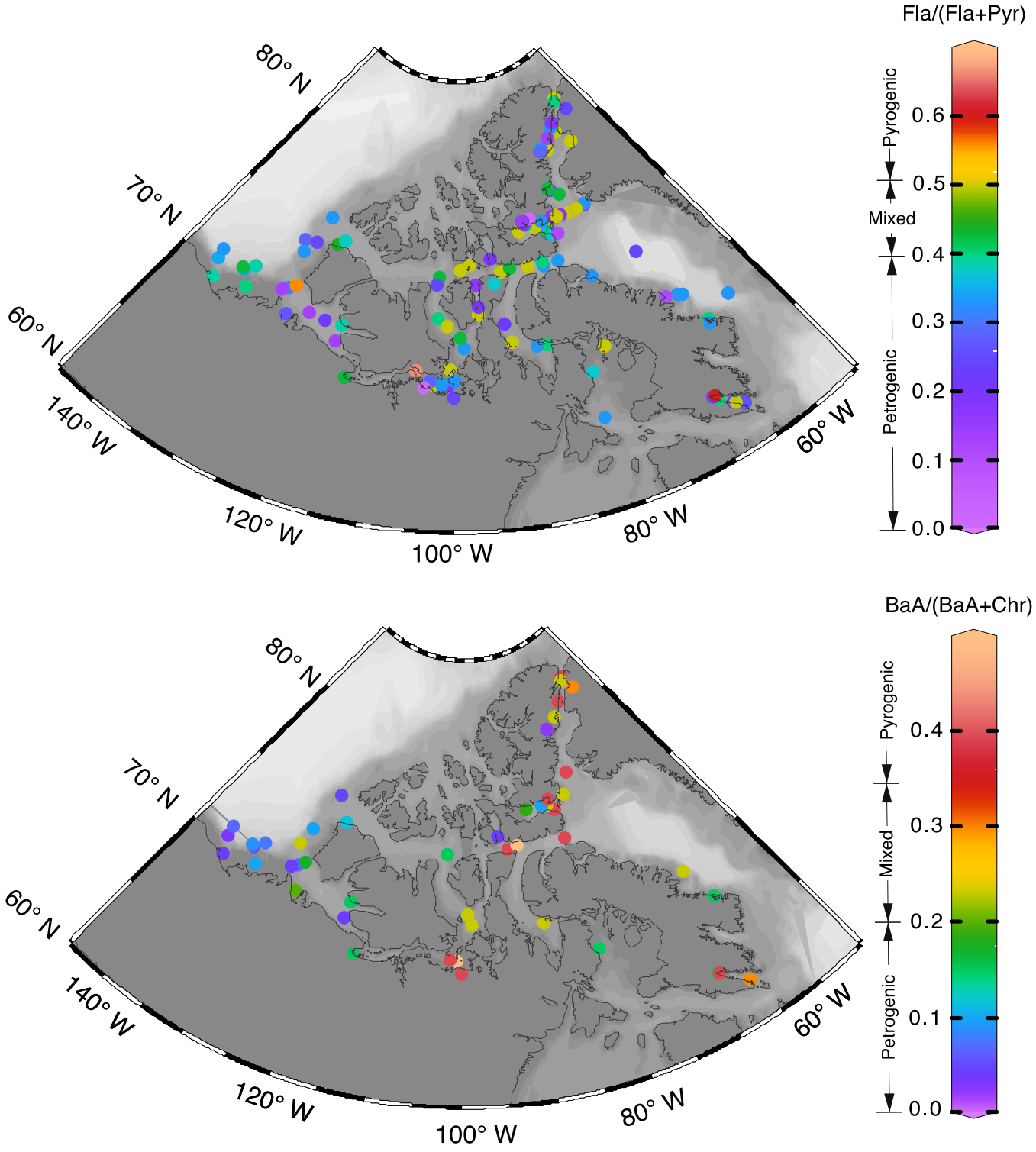

Fig. S6. Spatial distribution of Fla/(Fla+Pyr) and BaA/(BaA+Chr) in the CAA sediments.

Table S1. Comparison of the spike-corrected recoveries for certified reference material NIST-1944 between this study and the reference study of Choi *et al.* (2014).

Compound	**Mean recovery value (%) for this study (n=20)**	**Mean recovery value (%) for the reference study**
Naphthalene	31.8	46.1
1-Methylnaphthalene	66.6	65.4
2-Methylnaphthalene	30.2	50.5
Acenaphthene	37.2	56.1
Fluorene	38.0	34.1
Phenanthrene	86.6	82.4
Anthracene	75.7	56.6
Fluoranthene	88.6	95.3
Pyrene	78.4	80.9
Benz(a)anthracene	67.8	69.9
Chrysene	83.8	84.7
Benzo(b)fluoranthene	82.7	82.7
Benzo(k)fluoranthene	70.1	73.6
Benzo(a)pyrene	66.2	10.0
Indeno(1,2,3-c,d)pyrene	29.8	91.3
Dibenz(a,h)anthracene	121.7	145.0
Benzo(g,h,i)perylene	62.1	101.0

Table S2. Method detection limit (MDL) calculated based on the 7 replicates.

Compound	1	2	3	4	5	6	7	Standard deviation	MDL ug/mL (x 3.143)	MDL ng/g
Naphtalene	0.47	0.41	0.47	0.49	0.52	0.50	0.52	0.0353	0.111	63.5
1-Methylnaphthalene	0.43	0.35	0.46	0.46	0.51	0.49	0.50	0.0506	0.159	90.9
1-Methylnaphthalene-d10	0.11	0.09	0.13	0.12	0.12	0.14	0.13	0.0151	0.048	27.2
2-Methylnaphthalene	0.47	0.36	0.50	0.49	0.50	0.46	0.51	0.0478	0.150	85.9
2,6-Dimethylnaphthalene	0.09	0.09	0.11	0.12	0.12	0.13	0.12	0.0146	0.046	26.2
Acenaphthylene	0.85	0.74	0.89	0.88	1.02	0.97	0.97	0.0868	0.273	155.9
Acenaphthene	0.44	0.35	0.44	0.45	0.50	0.48	0.46	0.0440	0.138	79.1
2,3,5-Trimethylnaphthalene	0.11	0.10	0.12	0.10	0.12	0.11	0.12	0.0083	0.026	15.0
Fluorene	0.09	0.07	0.09	0.09	0.10	0.09	0.09	0.0083	0.026	15.0
Phenanthrene	0.05	0.03	0.05	0.04	0.04	0.05	0.05	0.0073	0.023	13.1
Anthracene	0.04	0.03	0.05	0.05	0.05	0.04	0.05	0.0073	0.023	13.1
1-Methylphenanthrene	0.11	0.09	0.12	0.12	0.12	0.11	0.13	0.0118	0.037	21.2
3,6-Dimethylphenanthrene	0.12	0.08	0.11	0.12	0.11	0.11	0.11	0.0125	0.039	22.4
Fluoranthene	0.16	0.12	0.15	0.18	0.18	0.17	0.17	0.0196	0.062	35.2
Pyrene	0.02	0.02	0.02	0.02	0.05	0.04	0.03	0.0112	0.035	20.2
9,10-Dimethylanthracene	0.10	0.08	0.10	0.08	0.12	0.11	0.12	0.0155	0.049	27.9
Benz(a)anthracene-d12	0.07	0.05	0.07	0.08	0.09	0.06	0.07	0.0120	0.038	21.5
Benz(a)anthracene	0.03	0.02	0.03	0.03	0.03	0.02	0.03	0.0045	0.014	8.1
Chrysene	0.03	0.02	0.03	0.03	0.05	0.03	0.04	0.0088	0.028	15.8
Benzo(b)fluoranthene	0.03	0.03	0.04	0.03	0.04	0.05	0.06	0.0107	0.034	19.2
Benzo(k)fluoranthene	0.03	0.01	0.02	0.02	0.01	0.03	0.02	0.0076	0.024	13.6
Benzo(a)pyrene	0.01	0.01	0.02	0.02	0.01	0.02	0.02	0.0049	0.016	8.9
Indeno(1,2,3-c,d)pyrene	0.02	0.02	0.03	0.03	0.03	0.02	0.03	0.0049	0.016	8.9
Dibenz(a,h)anthracene	0.03	0.03	0.05	0.05	0.04	0.03	0.04	0.0083	0.026	15.0
Benzo(g,h,i)perylene	0.07	0.03	0.06	0.05	0.05	0.04	0.03	0.0139	0.044	24.9

Table S3. Content range (ng g^{-1}, dw) for each PAH.

Compound	Surficial sediments			Terrestrial Sediments	Core Sediments
	Western Archipelago	Central Archipelago	Eastern Archipelago		
Naphthalene	3.0 - 27.2 (14.5)	ND - 8.0 (4.2)	1.5 - 3.8 (4.1)	3.9 - 20.5 (8.8)	0.0 - 13.7 (4.6)
1-Methylnaphthalene	4.4 - 52.0 (24.5)	ND - 13.9 (3.8)	0.0 - 8.0 (3.3)	2.0 - 17.9 (6.7)	0.0 - 22.7 (4.3)
2-Methtlnaphthalene	3.0 - 36.1 (19.3)	ND - 9.9 (2.5)	0.0 - 8.6 (2.6)	2.0 - 13.4 (5.9)	0.0 - 22.1 (3.9)
2,6-Dimethylnaphthalene	2.3 - 26.0 (12.0)	0.0 - 5.6 (1.8)	0.0 - 14.7 (2.5)	0.0 - 6.7 (2.2)	0.0 - 15.9 (3.5)
Acenaphthylene	0.0 - 3.0 (1.1)	ND	ND - 1.5 (0.1)	0.0 - 2.2 (0.2)	0.0 - 0.3 (0.3)
Acenaphthene	1.2 - 9.1 (4.2)	0.0 - 7.4 (2.0)	0.0 - 7.5 (1.8)	0.0 - 2.2 (0.6)	0.0 - 5.9 (1.0)
2,3,5-Trimethylnaphthalene	1.0 - 23.1 (8.0)	0.0 - 6.0 (1.2)	ND - 25.1 (2.5)	0.0. - 4.5 (1.0)	0.0 - 22.7 (4.2)
Fluorène	0.0 - 23.7 (6.2)	0.0 - 7.0 (1.5)	0.0 - 13.9 (2.8)	0.0 - 11.2 (2.5)	ND - 12.1 (3.0)
Phenanthrene	8.9 - 63.5 (33.3)	2.3 - 23.8 (8.7)	0.0 - 33.3 (9.5)	0.0 - 10.1 (3.7)	ND - 61.2 (13.0)
Anthracene	1.2 - 7.8 (2.8)	ND - 8.9 (1.6)	0.0 - 8.3 (1.4)	ND - 9.0 (1.8)	ND - 4.5 (1.0)
1-Methylphenanthrene	2.3 - 30.5 (9.4)	0.0 - 11.9 (2.7)	ND - 11.6 (2.1)	0.0 - 20.1 (4.1)	ND - 14.4 (3.4)
3,6-Dimethylphenanthrene	1.5 - 21.7 (7.6)	0.0 - 9.9 (3.1)	0.0 - 14.9 (2.8)	0.0 - 58.2 (7.7)	0.0 - 17.0 (3.0)
Fluoranthene	0.0 - 23.7 (1.2)	1.2 - 9.0 (3.2)	0.0. - 19.9 (4.1)	0.0 - 40.3 (6.0)	0.0 - 28.4 (5.6)
Pyrene	4.1 - 30.7 (15.8)	0.0 - 18.5 (8.0)	1.4 - 79.5 (8.0)	2.8 - 205.9 (27.2)	ND - 81.3 (9.6)
9,10-Dimethylanthracene	0.0 - 13.8 (5.2)	0.0 - 13.4 (3.6)	0.0 - 14.4 (2.7)	1.9 - 17.6 (6.4)	0.0 - 14.3 (3.3)
Benz(a)anthracene	ND - 7.8 (4.2)	ND - 2.5 (0.5)	ND - 3.9 (0.9)	ND - 6.0 (1.1)	ND - 16.3 (1.5)
Chrysene	2.9 - 42.2 (18.1)	0.0 - 11.4 (2.4)	0.0 - 19.1 (2.7)	0.0 - 30.0 (5.9)	ND - 22.1 (5.3)
Benzo(b)fluoranthene	ND - 18.2 (4.3)	ND - 7.1 (0.7)	ND - 40.6 (2.2)	ND - 18.3 (6.8)	ND - 10.1 (1.6)
Benzo(k)fluoranthene	ND - 17.4 (3.7)	ND - 5.7 (0.7)	0.0 - 4.8 (0.9)	ND - 2.6 (0.6)	ND - 13.6 (2.4)
Benzo(a)pyrene	0.0 - 96.7 (8.5)	0.0 - 34.2 (1.6)	0.0 - 48.5 (4.0)	0.0 - 11.0 (2.3)	0.0 - 29.8 (5.3)
Indeno(1,2,3-c,d)pyrene	0.0 -6.3 (2.4)	ND - 1.5 (0.1)	ND - 1.7 (0.2)	ND - 1.5 (0.2)	ND - 3.7 (0.4)
Dibenz(a,h)anthracene	0.0 - 6.3 (2.4)	0.0 - 1.5 (0.1)	ND - 1.2 (0.0)	0.0 - 11.0 (1.7)	ND - 3.7 (0.3)
Benzo(g,h,i)perylene	0.0 -22.5 (9.7)	0.0 - 7.6 (0.9)	ND - 4.0 (1.2)	ND - 10.5 (1.5)	ND - 22.2 (2.1)

Note: in parentheses are the mean values.

Table S4. Variance in the samples explained and loadings of the three significant factors determined via PCA.

Compounds	PC1 24%	PC2 15%	PC3 14%
Naphthalene	0.07	0.01	0.19
1-Methylnaphthalene	-0.14	0.13	0.43
2-Methylnaphthalene	-0.17	0.17	0.42
2,6-Dimethylnaphthalene	-0.36	0.02	0.11
Acenaphthene	0.14	-0.59	0.36
2,3,5-Trimethylnaphthalene	-0.58	-0.03	-0.34
Fluorene	-0.27	-0.33	-0.34
Phenanthrene	-0.08	-0.08	-0.17
Anthracene	0.18	-0.35	0.10
1-Methylphenanthrene	0.19	0.20	-0.10
3,6-Dimethylphenanthrene	0.26	0.05	-0.10
Fluoranthene	0.12	0.11	-0.30
Pyrene	0.26	0.17	-0.15
9,10-Dimethylanthracene	0.40	-0.03	-0.22
Chrysene	-0.02	0.53	0.11

Note : green indicates the 3 highest positive loadings; red indicates the 3 highest negative loadings